Definition and benchmarking of ab initio fragment methods for accurate excimer potential energy surfaces

Bónis Barcza,[†,¶] Ádám B. Szirmai,[†,¶] Attila Tajti,[†] John F. Stanton,[‡] and Péter G. Szalay[*,†]

†*Laboratory of Theoretical Chemistry, Institute of Chemistry, Eötvös University, P. O. Box 32, H-1518, Budapest 112, Hungary*

‡*Quantum Theory Project, Department of Chemistry, University of Florida, Gainesville, Florida 32611, United States*

¶*György Hevesy Doctoral School, ELTE Eötvös Loránd University, Institute of Chemistry*

E-mail: szalay@chem.elte.hu

Abstract

While Coupled-Cluster methods have been proven to provide an accurate description of excited electronic states, the scaling of the computational costs with the system size limits the degree for which these methods can be applied. In this study a fragment-based approach is presented for non-covalently bound molecular complexes with interacting chromophores of the fragments (so called *Frenkel pairs*), such as π-stacked nucleobases.

The interaction of the fragments is considered at two distinct steps. First, the states localized on the fragments are described in the presence of the other fragment(s); for

this we test two approaches. One method is founded on QM/MM principles, only including the electrostatic interaction between the fragments in the electronic structure calculation with Pauli repulsion and dispersion effects added separately. The other model, a Projection-based Embedding (PbE) using the Huzinaga equation includes both electrostatic and Pauli repulsion and only needs to be augmented by dispersion interactions. In both schemes the extended Effective Fragment Potential (EFP2) method of Gordon *et al.* was found to provide an adequate correction for the missing terms.

In the second step, the interaction of the localized chromophores is modeled for a proper description of the excitonic coupling. Here the inclusion of purely electrostatic contributions appears to be sufficient: it is found that the Coulomb part of the coupling, as evaluated by the transition density cube method, provides accurate splitting of the energies of interacting chromophores that are separated by more than 4 Å.

Keywords: excited states, exciton coupling, intermolecular interactions, Effective Fragment Potential, Pauli repulsion, embedding, QM/MM, dispersion ■

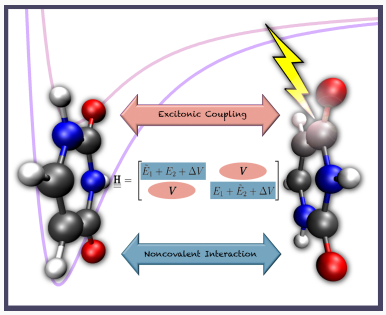

QM/MM and projector-based embedding schemes using CCSD electronic structure calculations are formulated and tested for non-covalent complexes of bi-chromophor systems

1 Introduction

Recent decades witnessed significant development of quantum chemical methodology; larger and larger molecules can be treated with increasing accuracy and, at the same time, the need for calculations to support experimental observations is becoming more relevant. For the electronic ground state well established methods are available and quantum chemistry, often by density functional theory (DFT), is able to study structures and even reactions of molecules as large as polypeptides. However, many important problems cannot be treated with ground state methods. These involve, for example, electron transfer between distant regions in biomolecules or situations associated with electronic excitations affecting multiple local domains. Since established methods cannot describe such processes, the demand for new tools to treat excited states in large systems is increasing.

There are two possible routes towards this goal. One option is to develop new approximate methods, but maintaining the accuracy and reliability is not a trivial task.[1–5] Alternatively, one can aim at defining (multiscale) approaches where only the important part of the system is treated at the high level, while the rest is approximated at a lower level. Different types of embedding methods, like quantum mechanics/molecular mechanics (QM/MM),[6] "our own N-layered integrated molecular orbital and molecular mechanics" (ONIOM),[7] projector-based embedding (PbE),[8] frozen density embedding (FDE)[9,10] and local correlation methods[11–17] are available for describing many processes in large systems. However, non-local phenomena are poorly suited for these approaches since they often require too large active partitions in these calculations.

Such collective events can indeed be very important. For example, we have found[18] that excitations can be delocalized to at least four nucleobases in oligonucleotides. Indeed, this study left open the question of whether even more units play a role in excited states of RNA and DNA chains. For such situations fragment methods[19] could be the preferred approach, where several "active" centers can be handled at a high level of theory and the properties of the entire system are calculated from those of the individual fragments, considering proper coupling terms between them. Fragment methods are well suited for calculations of non-covalently bound systems, since the choice of fragmentation is obvious. From the point of

view of excited states, DNA is also one of such systems since the excitations do not delocalize anywhere but the nucleobases that interact in a non-covalent manner.[20]

Regarding the route towards developing such a fragment-based method, our previous work[21] investigated the possibilities of obtaining accurate ground state potential curves of non-covalent dimers using high-level Coupled Cluster (CC) methods applied to the electronic structure of the fragments. Several schemes have been tested and we have found that both QM/MM and PbE methods (with a proper account for dispersion and Pauli repulsion - "exchange interaction" - terms from the extended Effective Fragment Potential (EFP2)[22–24] model) are capable of reproducing full dimer calculations at the same level of theory with high fidelity. In this work, we take another step forward by extending this methodology to (singly) excited states, thereby considering multi-chromophore systems.

The general Hamiltonian of two interacting fragments is expressed as

$$\hat{H}(\mathbf{r}_1, \mathbf{r}_2) = \hat{H}_1(\mathbf{r}_1) + \hat{H}_2(\mathbf{r}_2) + \hat{V}_{1,2}(\mathbf{r}_1, \mathbf{r}_2), \tag{1}$$

with $\hat{H}_i$ being the Hamiltonian of the non-interacting fragments and $\hat{V}_{1,2}(\mathbf{r}_1, \mathbf{r}_2)$ that of their interaction. This Hamiltonian suggest a perturbative treatment with the product of the fragments' wavefunctions as zeroth order. When considering the ground state and one excited state on each fragment, the product wavefunctions take the form

$$\begin{aligned} \Psi_0(\mathbf{r}_1, \mathbf{r}_2) &= \Phi_{1,0}(\mathbf{r}_1)\Phi_{2,0}(\mathbf{r}_2) \\ \Psi_1(\mathbf{r}_1, \mathbf{r}_2) &= \Phi_{1,1}(\mathbf{r}_1)\Phi_{2,0}(\mathbf{r}_2) \\ \Psi_2(\mathbf{r}_1, \mathbf{r}_2) &= \Phi_{1,0}(\mathbf{r}_1)\Phi_{2,1}(\mathbf{r}_2), \end{aligned} \tag{2}$$

where the indices 1 and 2 refer to the two fragments. $\Phi_{i,k}$ is the kth eigenfunction of the Hamiltonian of fragment i:

$$\hat{H}_i(\mathbf{r}_i)\Phi_{i,k}(\mathbf{r}_i) = E_{i,k}\Phi_{i,k}(\mathbf{r}_i). \tag{3}$$

The interacting states of the entire system can be obtained by the so-called *exciton model* by diagonalizing the Hamiltonian in the three-dimensional space of the functions in Eqn. (2),

as first suggested by Frenkel,[25] later by Davydov[26] and used in many applications (see *e.g.* Refs. 27–29 and references therein).

The quality of such a perturbative approach depends on the strength of the coupling. A fraction of their effects can be captured by repartitioning the Hamiltonian of Eqn. (1):

$$\hat{H}(\mathbf{r}_1, \mathbf{r}_2) \;=\; \hat{H}_1^{eff}(\mathbf{r}_1; \mathbf{r}_2) + \hat{H}_2(\mathbf{r}_2) + \Delta V_1(\mathbf{r}_1, \mathbf{r}_2), \tag{4}$$

where $\hat{H}_1^{eff} = \hat{H}_1 + \hat{V}_1^{eff}$ and $\Delta V_1(\mathbf{r}_1, \mathbf{r}_2) \approx \hat{V}_{1,2}(\mathbf{r}_1, \mathbf{r}_2) - \hat{V}_1^{eff}$. $\hat{H}_1^{eff}$ is essentially an embedded Hamiltonian which can be used to describe the ground state and also local excited states in the presence of the other fragment. The accuracy of this approach will primarily depend on the choice of $\hat{V}_1^{eff}$ and $\Delta V_1(\mathbf{r}_1, \mathbf{r}_2)$; several variants have been tested in our previous study.[21] This formalism can also be applied to the excited state of the complex, provided the excitation is localized on one fragment (see *e.g.* Ref. 30).

In the present study this scheme is extended to interacting chromophores by applying the exciton model; after obtaining the fragment energies and wavefunctions of the effective Hamiltonians ($\hat{H}_i^{eff}$), the resulting excited states are obtained by diagonalizing the Hamiltonian matrix defined in the space of the two locally excited product functions.

The scheme suggested here has thus two main ingredients. First, a proper definition of the effective Hamiltonian $\hat{H}_i^{eff}$ is needed, which includes the intermolecular interactions compatible with the electronic structure method that is used. Eventually, a corresponding ΔV_i is necessary to include the missing interaction terms. Based on our experience with the ground state,[21] QM/MM and PbE approaches used with Coupled Cluster (CC) electronic structure methods, augmented with EFP2 dispersion and Pauli repulsion[22–24] are able to describe the interaction of the fragments properly, and are worthwhile of generalization to excited states. Second, an appropriate approximation for the excitonic or Frenkel coupling between the excited states also needs to be established.

Similar methods have been suggested, among others, by Morrison *et al.*,[27] Sisto *et al.*,[28] Amadei *et al.*,[29] and Head-Gordon *et al.*[31] The novelty of the schemes presented here is the use of high-level CC theory for the electronic structure of the fragments and the careful selection of all components of the non-covalent interaction energy.

Obtaining proper reference data for validation of the models turns out to be a non-trivial task. Problems arise from converging the calculations to the proper states (in particular when diffuse basis functions are used), from the presence of charge transfer (CT) type electronic states in the low-energy spectrum at small intermolecular distances, as well as from the choice of counterpoise correction (CP) in excited states. The present study will also address these issues.

The paper is organized as follows. Section 2 gives a short summary of the available methodologies, with emphasis on the differences in theoretical formulations and the possibility of incorporating them into *ab initio* calculations. Section 3 presents the molecular systems used in the tests. Section 4 describes the computational details, while the results and discussion are presented in Section 5.

2 Methodologies for modeling intermolecular interactions in excited states

Let us introduce the proposed methodology on the simplest example of a supersystem consisting of two fragments, with just one excited state considered on both. To describe the Frenkel coupling of the two excitations localized on the fragments, we select product functions describing the two, locally excited states:

$$\begin{aligned} \tilde{\Psi}_1(\mathbf{r}_1,\mathbf{r}_2) &= \tilde{\Phi}_{1,1}(\mathbf{r}_1)\Phi_{2,0}(\mathbf{r}_2) \\ \tilde{\Psi}_2(\mathbf{r}_1,\mathbf{r}_2) &= \Phi_{1,0}(\mathbf{r}_1)\tilde{\Phi}_{2,1}(\mathbf{r}_2), \end{aligned} \tag{5}$$

where $\mathbf{r}_1$ and $\mathbf{r}_2$ represent the coordinates of fragment 1 and 2, respectively. The first function describes the excited state localized on the first fragment, while the second function describes the one localized on the second fragment, and they belong to two different partitionings of the Hamiltonian:

$$\begin{aligned} \hat{H}(\mathbf{r}_1,\mathbf{r}_2) &= \hat{H}_1^{eff}(\mathbf{r}_1;\mathbf{r}_2) + \hat{H}_2(\mathbf{r}_2) + \Delta V_1(\mathbf{r}_1,\mathbf{r}_2) \\ \hat{H}(\mathbf{r}_1,\mathbf{r}_2) &= \hat{H}_2^{eff}(\mathbf{r}_1;\mathbf{r}_2) + \hat{H}_1(\mathbf{r}_2) + \Delta V_2(\mathbf{r}_1,\mathbf{r}_2), \end{aligned} \tag{6}$$

where $\hat{H}_i^{eff}$ $\left(= \hat{H}_i + \hat{V}_i^{eff}\right)$ includes the effect of the environment through an "embedding potential" $\hat{V}_i^{eff}$. The fragment wavefunctions with a tilde ($\tilde{\Phi}_{1,1}(\mathbf{r}_1), \tilde{\Phi}_{2,1}(\mathbf{r}_2)$) are eigenfunctions of the corresponding effective Hamiltonians

$$\hat{H}_i^{eff}\tilde{\Phi}_{i,1} = \tilde{E}_{i,1}\tilde{\Phi}_{i,1} \tag{7}$$

and thus include the effect of the other fragment's ground state through $\hat{V}_i^{eff}$, while the corresponding unadorned ($\Phi_{1,1}(\mathbf{r}_1), \Phi_{2,1}(\mathbf{r}_2)$) are eigenfunctions of the unperturbed subsystems (see Eqn. (3)). The inclusion of the approximate "remaining potential" $\Delta V_i(\mathbf{r}_1, \mathbf{r}_2)$ $\left(\approx \hat{V}_{1,2}(\mathbf{r}_1, \mathbf{r}_2) - \hat{V}_i^{eff}\right)$ is necessary to correct for interactions which are not (or cannot be) accounted for when the eigenproblem of $\hat{H}_i^{eff}$ is solved (see later).

$\tilde{\Psi}_1(\mathbf{r}_1, \mathbf{r}_2)$ is a good approximation for locally excited states with energy

$$E_1 = \tilde{E}_{1,1} + E_{2,0} + \Delta V_1, \tag{8}$$

but does not include any polarization between the two fragments. This expression is often used in QM/MM and other embedding schemes; we also have tested it in Ref. 30. The quality of this approximation depends on the electronic structure method used, as well as upon the choice of $\hat{V}_i^{eff}$ and ΔV_i; this will be discussed in detail in Subsection 2.1. Note that the above formalism does not consider the anti-symmetrization of the wavefunctions, therefore the corresponding "Pauli repulsion" contribution should be appropriately included in ΔV_i.

To consider Frenkel[25] (or exciton) coupling of the two chromophores on the fragments, the matrix of the Hamiltonian in the basis of the functions in Eqn. (5) should be diagonalized, *i.e.*

$$\mathbf{H} = \begin{bmatrix} \tilde{E}_{1,1} + E_{2,0} + \Delta V_1 & \tilde{V}(1,2) \\ \tilde{V}(2,1) & E_{1,0} + \tilde{E}_{2,1} + \Delta V_2 \end{bmatrix} \tag{9}$$

with

$$\tilde{V}(1,2) \;=\; \langle\tilde{\Psi}_1(\mathbf{r}_1,\mathbf{r}_2)|\hat{H}(\mathbf{r}_1,\mathbf{r}_2)|\tilde{\Psi}_2(\mathbf{r}_1,\mathbf{r}_2)\rangle. \tag{10}$$

To evaluate this coupling, appropriate approximations need to be introduced as discussed in Subsection 2.3.

First, however, the multi-level approaches that can be applied for solving the eigenproblem of $\hat{H}_i^{eff}$, along with the appropriate choice for the "remaining potential" are reviewed in Subsections 2.1 and 2.2.

2.1 Definition of the effective Hamiltonian

In this study, as in Ref. 21, two approaches to define an effective Hamiltonian that can be used with CC methods are tested.

2.1.1 QM/MM

The multilevel scheme termed QM/MM (Quantum Mechanics/Molecular Mechanics)[6] revolves around the representation of the environment with point charges that usually reside on atomic sites, allowing the treatment of large complexes in a very economical manner. Within this scheme the effective Hamiltonian of Eqn. (6) $\left(H_1^{eff}\right)$ is given by

$$\hat{H}_1^{eff,\ QM/MM}(\mathbf{r}_1,\mathbf{r}_2) \;=\; \hat{H}_1(\mathbf{r}_1) + \hat{V}_1^{electrostatic}(\mathbf{r}_1;\mathbf{r}_2), \tag{11}$$

where $\hat{V}_1^{electrostatic}$ represents the Coulomb interaction of fragments 1 and 2, the latter represented *via* the partial charges. The main advantage of this scheme is its straightforward incorporation into any quantum chemical method (and code), so that it is widely applied.

There are various ways to define the point charges, several sets are available *e.g.* in traditional molecular force fields like AMBER[32,33] or CHARMM.[34] A more flexible parametrization can be achieved using atomic multipoles[35,36] as, *e.g.*, within the Effective Fragment Potential (EFP) framework.[37–39] In our previous paper on the ground state of non-covalently bound complexes[21] the CHELPG (CHarges from ELectrostatic Potentials using a Grid-

based) algorithm[40] was found to work well with CC methods. In the context of CHELPG, the partial charges at the atomic sites are fit to reproduce the electrostatic potential and some low-order electrostatic moments of the molecule calculated at any level of theory, hence the one used for the active fragment (*e.g.* CCSD) can also be applied. Unlike in methodologies used in most conventional force field methods, this way an accurate set of charges can be obtained from fundamental considerations, consistent with the *ab initio* spirit of the schemes.

One should realize, however, that the effective Hamiltonian in Eqn. (11) does not include important interaction terms, such as dispersion and Pauli exchange between the fragments. Thus, for accurate interaction energies also at short distances, the latter need to be added *a posteriori via* $\Delta V_1(\mathbf{r}_1;\mathbf{r}_2)$ (see Subsection 2.2).

2.1.2 Huzinaga embedding scheme

A more sophisticated consideration of the environment and its interactions can be achieved with multilevel quantum chemical embedding methods. Bottom-up frozen density embedding[9,10] and top-down projector-based embedding (PbE)[8] strategies are both available. The former is computationally less demanding as subsystems are treated separately, while the latter avoids the issues arising from the lack of orthogonality between subsystems. PbE was first introduced by Manby and Miller[8] who included an arbitrary level shift parameter in the Fock operator of the embedded subsystem, raising the energy of environment orbitals to near infinity. Orthogonality between subsystems can also be achieved by adapting the Huzinaga-equation[41] to the embedding problem[42] or *via* the projection scheme of Hoffmann and Khait.[43] PbE has been applied to the calculation of excited states with various goals in mind. Bennie *et al.*[44] improved the original PbE method by including the most important occupied orbitals of the environment in the excited state calculation. Parravicini and Jagau[45] studied ionization, electron attachment and electronic resonances, also applying the concentric virtual orbital localization scheme.[46] A benchmark study by Hégely *et al.*[47] compared various multilevel approaches including PbE for the calculation of excitation energies.

In the present study the embedding scheme of Hégely and co-workers,[42] based on the Huzinaga-equation, is chosen as the second approach for the description of the active frag-

ment. Embedding a fragment treated at the CC level of theory into the environment of the other fragment described using density funcional theory (DFT) requires the *a priori* definition of the active subsystem and the environment. Following a DFT calculation on the entire system, the occupied molecular orbitals (MOs) of the fragments are localized, resulting in the splitting of the density matrix into two parts $\mathbf{D}_1$ and $\mathbf{D}_2$. The localization can be extended to the virtual orbital space, reducing the computational cost of the CC calculations, as well as allowing a cleaner treatment of localized excited states by avoiding charge transfer contributions (see later). The SPADE (Subsystem Projected AO DEcomposition)[48] method offers a black-box way of localizing and partitioning the orbital space based on the difference of singular values in a singular value decomposition scheme, and can be applied to both occupied and virtual orbitals.

The Fockian of the active subsystem is

$$\tilde{\mathbf{F}}_1 \;=\; \mathbf{h} + \mathbf{G}^{\mathrm{HF}}[\tilde{\mathbf{D}}_1] + (\mathbf{G}^{\mathrm{DFT}}[\mathbf{D}_{1,2}] - \mathbf{G}^{\mathrm{DFT}}[\mathbf{D}_1]), \tag{12}$$

where $\mathbf{h}$ and $\mathbf{G}^{\mathrm{HF}}[\tilde{\mathbf{D}}_1]$ are the core Hamiltonian and the two-electron part of the Fockian of subsystem 1, respectively, while the remaining terms in Eqn. (12) give the embedding potential. $\tilde{\mathbf{D}}_1$ is the one-electron density of the embedded active subsystem reoptimized in a second Hartree-Fock calculation during which the orthogonality of the subsystems is ensured by solving the Huzinaga-equation with the orbitals of the environment kept frozen:

$$(\tilde{\mathbf{F}}_1 - \mathbf{S}\mathbf{P}_2\tilde{\mathbf{F}}_1 - \tilde{\mathbf{F}}_1\mathbf{P}_2\mathbf{S} + 2\mathbf{S}\mathbf{P}_2\tilde{\mathbf{F}}_1\mathbf{P}_2\mathbf{S})\tilde{\mathbf{C}}_1 \;=\; \mathbf{S}\tilde{\mathbf{C}}_1\tilde{\boldsymbol{\mathcal{E}}}_1, \tag{13}$$

where $\mathbf{S}$ is the overlap matrix of the atomic orbitals, $\mathbf{P}_2$ is the projector onto the environment orbitals and $\tilde{\mathbf{C}}_1$ is the MO coefficient matrix of the embedded orbitals whose orbital energies are in the diagonal matrix $\tilde{\boldsymbol{\mathcal{E}}}_1$. The orbitals obtained this way can be used in correlated wavefunction (WF) calculations for both ground and excited states.[30]

The energy ansatz of this method for WF-in-DFT embedding is

$$E_1^{\mathrm{WF-in-DFT}}[\Psi_1; \tilde{\mathbf{D}}_1, \mathbf{D}_1, \mathbf{D}_2] \;=\; E_{1,2}^{\mathrm{DFT}}[\mathbf{D}_{1,2}] - E_1^{\mathrm{DFT}}[\mathbf{D}_1] + E_1^{\mathrm{WFT}}[\Psi_1; \tilde{\mathbf{D}}_1, \mathbf{D}_1, \mathbf{D}_2], \tag{14}$$

where $E_{1,2}^{\mathrm{DFT}}$ is the DFT energy of the entire supersystem, E_1^{DFT} is that of the active fragment calculated using the localized supersystem orbitals and E_1^{WFT} is the WF energy of the embedded fragment. This energy ansatz is general, meaning that the ground and excited state energies differ only in the WF term that is calculated using the same embedding potential in both cases. This is the result of the frozen environment orbitals as they remain unrelaxed to changes in the active orbital space. Note that the Fockian here is constructed from similar principles as the effective Hamiltonian introduced in Eqn. (6), i.e. it includes the electronic embedding by the enviroment's density. It is also apparent from the energy expression (Eqn. (14)) that inter-subsystem interactions are retained from the original ground state supersystem calculation at the DFT level of theory. This means that not only the electrostatic interaction, but also the ground state Pauli repulsion is included in the final energy. Common DFT functionals are known to fail in giving a proper description of dispersion interactions, thus the latter is missing from this ansatz and has to be included separately.

The first term on the right side of Eqn. (14) can be formally divided into monomer energies calculated using the localized supersystem MOs and the interaction energy term:

$$E_{1,2}^{\mathrm{DFT}}[\mathbf{D}_{1,2}] \;=\; E_1^{\mathrm{DFT}}[\mathbf{D}_1] + E_2^{\mathrm{DFT}}[\mathbf{D}_2] + E_{1,2,\mathrm{int}}^{\mathrm{DFT}}[\mathbf{D}_{1,2}]. \tag{15}$$

Therefore, the original energy ansatz (Eqn. (14)) above contains the fragment energies at two different levels of approximation: that of the active fragment from the wavefunction calculation ($E_1^{\mathrm{WFT}}[\Psi_1;\tilde{\mathbf{D}}_1,\mathbf{D}_1,\mathbf{D}_2]$), while the fragment playing the role of environment is treated at the DFT level ($E_2^{\mathrm{DFT}}[\mathbf{D}_2]$). This results in an incorrect asymptotic behavior of relative energy curves for non-homodimer systems. Therefore, we suggest the use of a modified energy expression:

$$\begin{aligned}
\bar{E}_1^{\mathrm{WF-in-DFT}} &= E_1^{\mathrm{WF-in-DFT}}[\Psi_1;\tilde{\mathbf{D}}_1,\mathbf{D}_1,\mathbf{D}_2] + E_2^{\mathrm{WF-in-DFT}}[\Psi_2;\tilde{\mathbf{D}}_2,\mathbf{D}_1,\mathbf{D}_2] - E_{1,2}^{\mathrm{DFT}}[\mathbf{D}_{1,2}], \\
&= E_1^{\mathrm{WFT}}[\Psi_1;\tilde{\mathbf{D}}_1,\mathbf{D}_1,\mathbf{D}_2] + E_2^{\mathrm{WFT}}[\Psi_2;\tilde{\mathbf{D}}_2,\mathbf{D}_1,\mathbf{D}_2] + E_{1,2,\mathrm{int}}^{\mathrm{DFT}}[\mathbf{D}_{1,2}].
\end{aligned} \tag{16}$$

2.2 Choice of the remaining potential ΔV_i

The schemes above lack some important intermolecular interactions: *QM/MM* does not include any van der Waals type interactions, while dispersion is missing from the PbE approach. Based on our findings in Ref. 21, correcting for dispersion and Pauli repulsion *via* the $\Delta V_1(\mathbf{r}_1, \mathbf{r}_2)$ term in the Hamiltonian is an appropriate approximation and the extended Effective Fragment Potential (EFP2) developed by Gordon and coworkers[22–24,49–51] is an excellent choice. (See Ref. 21 for other possibilities.)

The essence of the EFP2[22] is that an adequate parameter set for the potential is derived from first principle considerations. The algorithm is able to predict every important contribution to the intermolecular interactions, but here we shortly discuss only the Pauli repulsion and dispersion terms, which are used in the calculations. For a more detailed description of the EFP2 formalism, the reader is referred to Refs. 23, 24, 51.

To obtain the dispersion contribution in EFP2,[52] a set of points are defined in the first step, located at the nuclear positions and the midpoints of covalent bonds. These serve as the centers of localized molecular orbitals (LMO) obtained from a HF or DFT calculation of the subsystem. Then the dynamic dipole polarizabilities around the centroids of these LMOs are determined by applying the time-dependent extension of the chosen method, which are then used to calculate the dispersion energies between the fragments. Additional damping parameters derived from the overlap of these orbitals are also used to correct the behavior at short separations.

For the Pauli repulsion in the EFP2 scheme,[24] the necessary antisymmetrization is achieved by restricting the permutations to just two electrons and approximating the energetic effect with a power series with respect to the orbital overlaps (S). The terms beyond $\mathcal{O}(S^3)$ are neglected, while additional simplifications are applied also to the lower-order terms.

According to the literature,[53,54] EFP2 is a good model for interactions of molecules in the ground state. However, to our knowledge, only one attempt has been made to treat excited states with EFP2: Rojas and Slipchenko[55] calculated the solvent effect on the excitation energies of nine chromophores. In this study, the Pauli repulsion term was included in the

effective Hamiltonian (so called QM/EFP2 scheme).[56,57] Important efforts have also been made by Hapka, Przybytek, and Pernal[58,59] to include the dispersion between the ground and excited states within SAPT (Symmetry-Adapted Perturbation Theory).[60,61] These methods are not yet available for routine applications.

Therefore, since the experience with the ground state clearly reveals that dispersion and Pauli repulsion are necessary to achieve the accuracy we aim at,[21] we decided to check whether the ground state corrections are also applicable to the excited states. Note that this is a common practice in TD-DFT studies on excited states of non-covalent complexes.[62] The hope is that the error made this way is significantly smaller than the one completely neglecting these terms would introduce. This idea is supported by the fact that in excited states dominated by a single substitution, only a small fraction of the electrons are affected by the excitation and the dominant part of the electron density is similar in the ground and excited states. Although the results below show that this approximation works reasonably well, we hope that the success of the whole scheme presented in this paper will inspire research that will enable us to remove this restriction in the future.

To summarize, two, conceptually different methods will be used in the present study. One is a QM/MM approach based on CHELPG point charges, augmented with (ground state) dispersion and Pauli repulsion from EFP2 (termed as *QM/MM + EFP2* hereafter), while the other one is a Huzinaga projection based embedding model (PbE) augmented with an EFP2 (ground state) dispersion contribution (termed as *PbE + EFP2*).

2.3 Coupling schemes

The off-diagonal elements of the Hamiltonian matrix (Eqn. (10)) represent the coupling between excitations of the different chromophore groups. To consider possible approximations for $\tilde{V}(1,2)$, let us use the original partitioning of the Hamiltonian (Eqn. (1)) which treats both fragments equivalently. With this Hamiltonian, it is more reasonable to use the unbiased basis (Eqn. (2)) for the evaluation of the matrix elements. This approximation is not so severe since, presumably, the non-covalent interactions considered do not substantially

change the fragment wavefunctions. This means that

$$\begin{aligned}\tilde{V}(1,2) \approx V(1,2) &= \langle \Phi_{1,1}(\mathbf{r}_1)\Phi_{2,0}(\mathbf{r}_2)|\hat{H}_1(\mathbf{r}_1) + \hat{H}_2(\mathbf{r}_2) + \hat{V}_{1,2}(\mathbf{r}_1,\mathbf{r}_2)|\Phi_{1,0}(\mathbf{r}_1)\Phi_{2,1}(\mathbf{r}_2)\rangle \\ &= \langle \Phi_{1,1}(\mathbf{r}_1)\Phi_{2,0}(\mathbf{r}_2)|\hat{V}_{1,2}(\mathbf{r}_1,\mathbf{r}_2)|\Phi_{1,0}(\mathbf{r}_1)\Phi_{2,1}(\mathbf{r}_2)\rangle, \end{aligned} \quad (17)$$

i.e. the coupling is just the matrix element of the interaction potential $\hat{V}_{1,2}(\mathbf{r}_1,\mathbf{r}_2)$.

A simple way to calculate this term is to approximate the potential by the dipole approximation, first suggested by Förster[63]

$$\hat{V}_{1,2}(\mathbf{r}_1,\mathbf{r}_2) \approx \frac{\hat{\boldsymbol{\mu}}_1(\mathbf{r}_1)\cdot\hat{\boldsymbol{\mu}}_2(\mathbf{r}_2)}{R_{1,2}^3} - 3\frac{(\hat{\boldsymbol{\mu}}_1(\mathbf{r}_1)\cdot\mathbf{R}_{1,2})\ (\hat{\boldsymbol{\mu}}_2(\mathbf{r}_2)\cdot\mathbf{R}_{1,2})}{R_{1,2}^5}, \quad (18)$$

where $\mathbf{R}_{1,2}$ is the vector connecting the center-of-mass (COM) of the two choromophores, R_{12} is the distance between them, and $\hat{\boldsymbol{\mu}}_i(\mathbf{r}_i)$ is the dipole operator of fragment i.

With this approximation, the coupling can be calculated from the transition dipoles of the fragments:

$$V(1,2) = \frac{\boldsymbol{\mu}_1^{10}\boldsymbol{\mu}_2^{01}}{R_{12}^3} - 3\frac{(\boldsymbol{\mu}_1^{10}\cdot\mathbf{R}_{12})(\boldsymbol{\mu}_2^{01}\cdot\mathbf{R}_{12})}{R_{12}^5}, \quad (19)$$

with

$$\boldsymbol{\mu}_i^{kl} = \langle \Phi_{i,k}(\mathbf{r}_i)|\hat{\boldsymbol{\mu}}_i(\mathbf{r}_i)|\Phi_{i,l}(\mathbf{r}_i)\rangle.$$

This approach (called the *Transition Dipole Approximation (TrDA)* hereafter) is a simple and economical way to estimate the coupling. Note that the second term in Eq. 19 is needed only if the two transition dipole moments are not parallel, *i.e.* it gives no contribution in the stacked systems we investigate here.

The dipole approximation can be extended by considering transition monopoles *e.g.* at atomic centers[64] or by higher multipoles like in an extension of the PMM (Perturbed Matrix Method) approach (PMM-QQ).[65] However, Ref. 65 reveals that the extension in this form does not necessarily improve the accuracy of the coupling.

A more accurate approximation of $\hat{V}_{1,2}$ is to consider the exact Coulomb interaction

between the electrons of the two fragments

$$\hat{V}_{1,2}(\mathbf{r}_1, \mathbf{r}_2) = \sum_{i(1)} \sum_{j(2)} \frac{1}{|\mathbf{r}_i - \mathbf{r}_j|}, \tag{20}$$

where the indices ($i(1)$ and $j(2)$) run over the electrons of fragments 1 and 2, respectively. (The contribution of the nuclei to $\hat{V}_{1,2}$ vanishes in the commonly adopted Born-Oppenheimer and Condon approximations.[66]) With this, the coupling becomes:

$$\begin{aligned} V_{1,2} &= \int d\mathbf{r}_1 \, d\mathbf{r}_2 \; \Phi_{1,1}(\mathbf{r}_1)\Phi_{1,0}(\mathbf{r}_1) \; \hat{V}_{1,2}(\mathbf{r}_1, \mathbf{r}_2) \; \Phi_{2,0}(\mathbf{r}_2)\Phi_{2,1}(\mathbf{r}_2) \\ &= \int d\mathbf{r}_1 \, d\mathbf{r}_2 \; \rho_1^{0\to1}(\mathbf{r}_1) \; \hat{V}_{1,2}(\mathbf{r}_1, \mathbf{r}_2) \; \rho_2^{0\to1}(\mathbf{r}_2), \end{aligned} \tag{21}$$

i.e. it can be calculated from the transition densities ($\rho_i^{0\to i}$) of the two fragments.[66,67]

Krueger and co-workers[67] suggested to evaluate this expression on a grid and named the procedure the Transition Density Cube (TDC) method,[67,68] and we will use this nomenclature in the following.

We have implemented the grid representation of transition densities in the CFOUR[69,70] program system. This enables the calculation (within the numerical accuracy) of the electronic Coulomb interaction between the fragments at any theoretical level for which the transition density is available.

There are also other attempts in the literature to include accurate couplings for Frenkel-type excitonic interaction with specific electronic structure methods: CIS by Herbert and co-workers,[27] TD-DFT by Martinez and co-workers,[71] Curutchet and Mennucci[72] as well as Head-Gordon and co-workers,[73] and CC2 and related methods by Fückel *et al.*[66] These often also include the exchange type (Dexter) coupling,[74] which is relevant only at very short intermolecular distances. Since the Dexter coupling is not available at the CCSD level, it could not be included here. However, from the results presented, the distance where this term becomes important can be deduced.

Note that the same coupling also appears in Electron Energy Transfer (EET) processes,[75] and many approximate schemes have been suggested to include it. An overview of these

techniques is beyond the scope of this paper, more detail can be found *e.g.* in Refs. 76, 77.

3 Molecular systems

To find the approximation most suitable for excited states of non-covalently interacting dimers of nucleobases, we investigate, as in our previous paper on the ground state,[21] bimolecular complexes of nitrogen–containing heterocycles: stacked pyrrole-pyrole dimer (denoted by *(Pyr)*$_2$ hereafter), and cytosine-uracil complex (*Cyt-Ura*). In addition, the homodimers of cytosine (*(Cyt)*$_2$) and uracil (*(Ura)*$_2$), as well as that of formaldehyde (*(*CH_2O*)*$_2$) are included to better understand trends. The test systems are shown in Fig. 1. In the discussion below, the "distance" of monomers refers to that between the centers of masses. All the complexes were investigated in a stacked (sandwich) structure, with oppositely oriented dipoles, except for the *(Pyr)*$_2$ where the symmetry was lowered by a 10^o in-plane rotation away from the C_{2h} structure. The equilibrium structures of the monomers (optimized at the MP2/6-31G* level) were taken from Ref. 78 and are documented in Tables S1-S4 of the *Supplementary material* along with the geometries of dimers at a representative distance in Tables S5-S9.

The performance of methods describing excitonic states, as it has also been pointed out recently by Hancock and Goerigk,[62] should not just be evaluated in single point calculations. Therefore, the tests presented here include potential curves along the intermolecular separation. Although the proposed methodology can be generalized to practically any number of states, in this first application we limit consideration to the interaction of just two states. These tests should provide a better understanding on how the different approximations work in the suggested scheme.

In order to investigate the interaction of just a pair of states, these need to be energetically well separated from other electronic states. It turned out that selecting such pairs is not an easy task, in particular in calculations with diffuse basis functions; Rydberg states appearing among the excited states of molecules with π electronic structure result in a high density of states with strong interactions between them. In addition, at short distances charge transfer (CT) states complicate the spectrum. Therefore, to find appropriate states for the

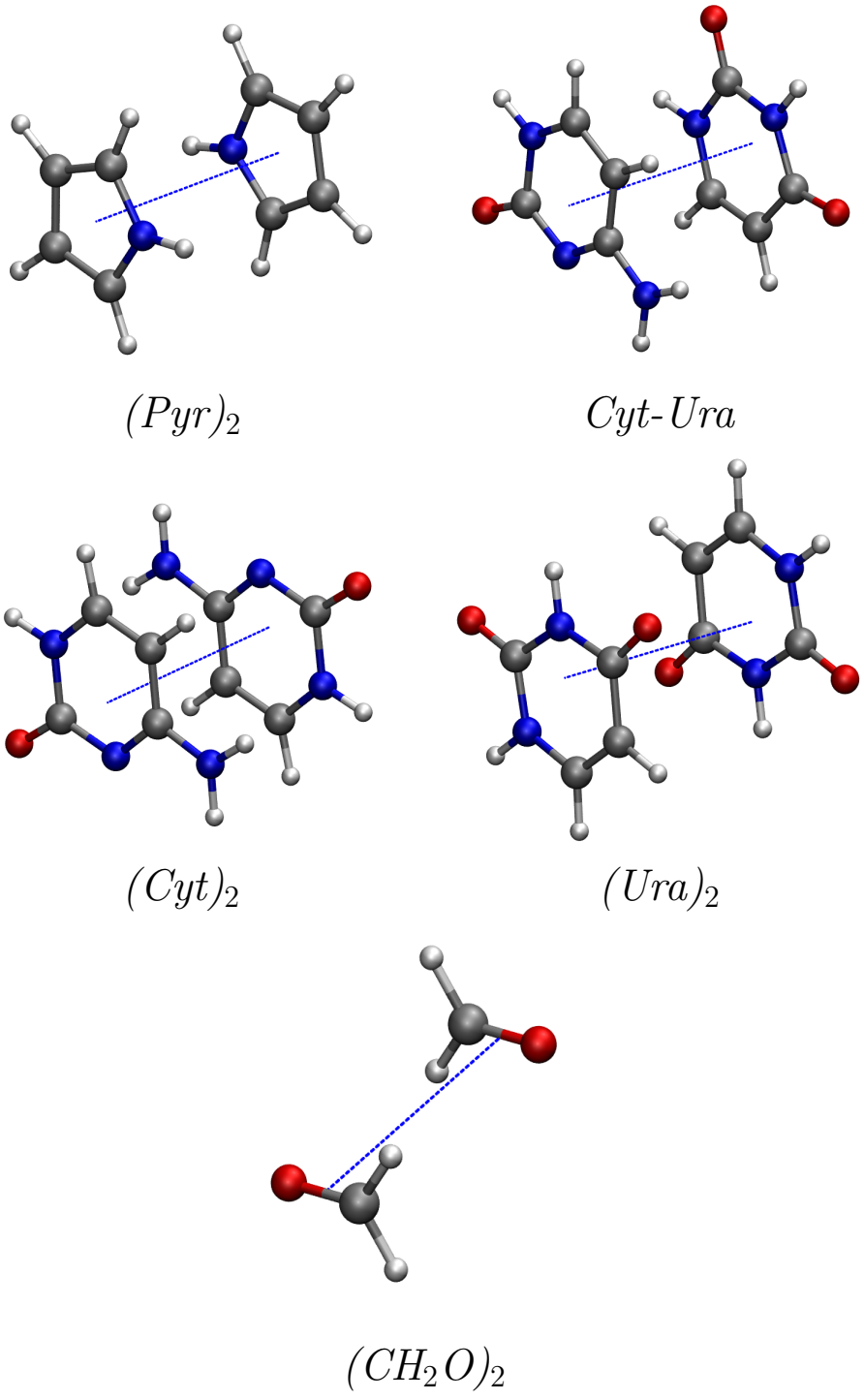

Figure 1: Orientation of the molecules in the test systems used in this study. The measure of the distance is represented by the blue dotted line connecting the centers of mass of the fragments.

tests, certain compromises were necessary, which will be be discussed later. The monomer electronic states considered in this study are summarized in Table 1.

Table 1: Summary of the monomer electronic states investigated in this study.

	Basis set	State	ΔE [a] / eV	f [b]
CH_2O	cc-pVDZ	$1\,^1A_1$ (ground)	0.00	
		$1\,^1B_1$ ($\sigma - \pi^*$)	9.36	0.002
		$2\,^1A_1$ ($\pi - \pi^*$)	9.95	0.011
CH_2O	aug-cc-pVDZ	$1\,^1A_1$ (ground)	0.00	
		$2\,^1A_1$ ($n - R$)	8.07	0.058
		$1\,^1B_1$ ($\sigma - \pi^*$)	9.24	0.001
		$3\,^1A_1$ ($\pi - \pi^*$)	9.59	0.166
Pyrrole	cc-pVDZ	$1\,^1A_1$ (ground)	0.00	
		$1\,^1B_2$ ($\pi - \pi^*$)	7.03	0.146
Pyrrole	aug-cc-pVDZ	$1\,^1A_1$ (ground)	0.00	
		$1\,^1B_1$ ($n - R$)	5.14	0.000
		$1\,^1A_2$ ($n - R$)	5.87	0.021
Cytosine	cc-pVDZ	$1\,^1$A' (ground)	0.00	
		$3\,^1$A' ($\pi - \pi^*$)	6.07	0.157
Uracil	cc-pVDZ	$1\,^1$A' (ground)	0.00	
		$2\,^1$A' ($\pi - \pi^*$)	5.78	0.199

[a] EOM-CCSD vertical excitation energies, in electron volts; [b] Oscillator strength evaluated at the EOM-CCSD level.

4 Computational details

The primary goal of developing fragment methods is to replace high level (Coupled Cluster (CC) type) electronic structure calculations on the complex with appropriately chosen calculations on the fragments. The family of CC-type methods allows systematic improvement of the accuracy, but approximate versions (like CC2[79] and ADC(2)[80] in particular with spin scaling[81,82]) enable an increase of the size of the fragments. Still, to avoid any ambiguity caused by the approximate methods, the first tests will be done with the Equation of Motion Coupled Cluster with Singles and Doubles (EOM-CCSD) method,[83,84] which can be performed not only for middle sized fragments considered in this work, but also for their complexes.

Double-zeta quality basis sets with diffuse functions have been selected for the calculations, giving a reasonable description of excited states and also of intermolecular interac-

tions[85] while making the corresponding EOM-CCSD calculations also feasible on the complexes. However, to be able to investigate valence $\pi - \pi^*$ excitations, the primary source for excimer states, some calculations had to be done without diffuse functions, even if the interaction energies obtained this way are clearly underestimated. One should proceed with great care when performing comparisons without diffuse functions, details are given below.

To summarize, all reference, QM/MM, and high-level steps of the PbE calculations were done with CCSD[86] and EOM-CCSD[83,84] level of theory in the frozen core approximation. Two basis sets were used in these calculations: cc-pVDZ[87] and aug-cc-pVDZ.[88] Only calculations using the same method and basis have been compared, allowing the evaluation of the fragment methods. Specific details of the calculations are discussed below.

4.1 Reference ab initio calculations

To assess the accuracy of a new scheme, appropriate comparison is necessary, which turned out to be a significant bottleneck of this study.

First, it was a major challenge to identify and converge valence excited states when diffuse functions were included in the basis due to the presence of interacting Rydberg states. This was not the case when the basis without diffuse functions was used. Clearly, this way just a limited portion of the interaction energy is captured, but with a careful selection of the parameters of the fragment calculations (see below) meaningful comparisons can be made.

Second, the calculations on the complex need to be corrected for basis set superposition error (BSSE) since the fragment calculations are free from this artificial lowering of the interaction energy. In our previous paper,[21] we used counterpoise correction (CP)[89] to correct the ground state energies of the complex. Although it is often claimed that CP corrections overestimate BSSE, particularly in correlated calculations,[90] it is still the state of the art in most studies of non-covalent interactions.[91] Note that the SNOOP method by Jorgensen *et al.*[92] is a noteworthy attempt to calculate a CP correction for correlated ground states, but requires special code which at present is only available in the LSDalton program suite.[93]

The definition of BSSE corrections for excited states is not obvious. Rocha-Rinza *et al.*[94] suggested the use of the CP correction formula analogous to the ground state one. This has

been used in some applications (see *e.g.* refs. 95, 96) but diffuse basis functions were not usually included in these calculations. Serrano-Andrés and Serrano-Pérez, in their review on excited states[97] suggested the use of the ground state CP correction also for the excited state due to the uncertainties of the above definition, particularly for delocalized situations. We have performed some test calculations applying the formula of Rocha-Rinza *et al.*,[94] the results are shown in Figure 2 for $(CH_2O)_2$ in aug-cc-pVDZ basis. While for some low-lying states the CP correction is similar to the ground state value at any distance, some states show unreasonably large CP corrections at close inter-fragment distances. A quick look into this problem revealed that the CP correction removes the charge transfer component of the solution, which is an artifact; many excited states of interacting fragments indeed have charge flow. Considering that CP correction is a basis set effect and mostly influences the orbitals,[90] the CP correction obtained at the HF level was used for both the ground state and the excited states. Note that this way the CP correction does not change the excitation energy, but does indeed influence the shape of the excited state energy surfaces. It is certainly worth investigating the problem in more detail, and such study is underway. Nevertheless, the present results indicate that this approximation is reasonable.

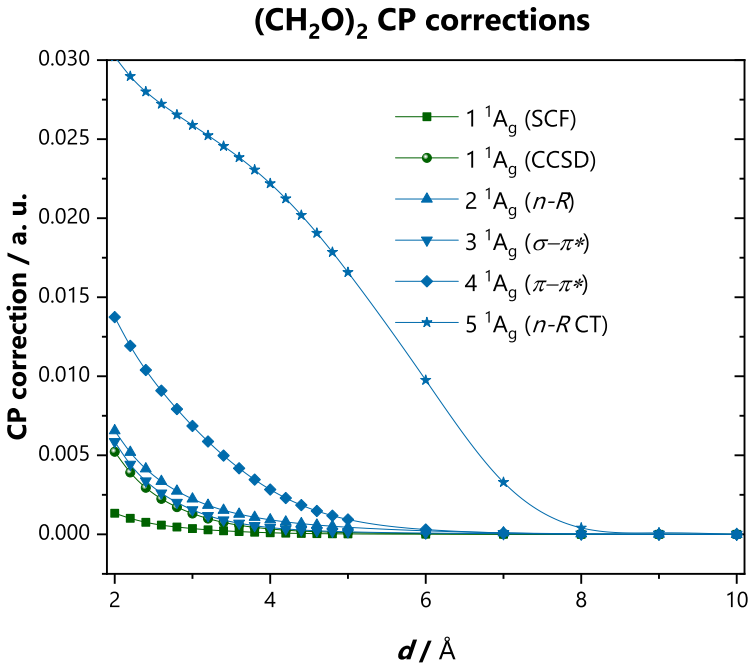

Figure 2: Counterpoise (CP) corrections calculated for several states of $(CH_2O)_2$.

All reference calculations have been performed using the CFOUR program package.[69,70]

4.2 Fragment calculations

The QM/MM calculations were performed at the same levels of theory as the reference calculations using CFOUR,[70] with the CHELPG point charges incorporated into the one-electron Hamiltonian.

The CHELPG point charges were obtained at the CCSD level using GAMESS[98] with the aug-cc-pVDZ basis set. Further details of the CHELPG calculations, as well as the determined atomic charges can be found in the *Supplementary material*.

The PbE calculations were performed using the MRCC program suite[99] with the resolution of the identity (RI) approximation applied for both the SCF and correlation components of the calculations. The active subsystem was treated at the same level as the reference and PBE functional[100] was used for the low level method. The localization and partitioning of the occupied and virtual orbital spaces was done by SPADE.[48] The energy expression of Eqn. (16) was used as the diagonal term in the Frenkel matrix. For all systems the PbE calculations used localized virtual orbitals; otherwise the excited state spectrum was spoiled by artifactual CT states. However, the $(CH_2O)_2$ dimer was also investigated using the full virtual space (in ground state calculation), as well as an extended SPADE-localized virtual space containing two additional orbitals to test the incorrect behavior of the method with diffuse basis functions (see Section 5.2).

The EFP2 dispersion and Pauli repulsion potentials were determined from the restricted Hartree-Fock wave function using the built-in routine of GAMESS[98] with the default settings as described in the manual of the program package.[101] The basis sets for these calculations were adjusted to the electronic structure calculations. For the augmented basis tests these interaction terms were calculated with the 6-311++G(3df,2p) basis set as suggested by Slipchenko and Gordon.[102] On the other hand, to compare with the reference results obtained with the cc-pVDZ basis, which clearly includes only a smaller portion of the interaction energy, the EFP2 parameters were also obtained with this non-augmented basis set. It will be checked below whether the EFP2 scheme gives reasonable interaction energies in this case.

4.3 Calculation of interstate couplings

The transition moments and transition densities of the investigated excited states were determined from monomer calculations on the same level as the reference calculations using CFOUR.[70] In the TDC scheme the transition densities were represented on a COM-centered grid of stepsize 0.25 Å with maximum dimension of 16x20x24 Å for formaldehyde and 20x20x20 Å for all other monomers corresponding to the Cartesian coordinates given in Tables S1-S4 in the *Supplementary material*. The numerical accuracy of the TDC procedure was evaluated by integrating the transition density for the entire space, as well as by comparing the transition moment obtained on the grid with that from the EOM-CC calculation.

Due to the bi-orthogonality of the CC framework, the above schemes need further adjustment. There are (slightly) different left and right transition properties which would result in slightly different interaction energies. Following the procedure that the physically relevant oscillator strength is calculated from the product of left and right transition dipoles, we use the geometric mean of the left and right transition properties to evaluate the coupling.

5 Results and discussion

In this section the different approximations defining our scheme are tested. The validity of approximations of the interaction energy is investigated in Section 5.1, the performance of different coupling schemes is presented in Section 5.3, while the final results, i.e. the total PESs of both states in question, are evaluated in Section 5.1.2. In addition, in Subsection 5.2 the problem related to the virtual space localization of the PbE scheme is discussed.

5.1 Interaction energy

5.1.1 Ground states

First, we review the quality of the ground state interaction potentials, including the EFP2 contributions, for the setups used later in the excited state calculations. In Figure 3 relative potential energy curves of the ground states of the $(CH_2O)_2$ and $(Pyr)_2$ dimers are shown, obtained with the aug-cc-pVDZ basis set. In the case of $(CH_2O)_2$, good agreement can

be observed for the *QM/MM + EFP2* curve, the difference to the reference getting clearly noticeable only at very short distances close to the equilibrium. The discrepancy seems to be larger for $(Pyr)_2$.

On the other hand, the *PbE + EFP2* curves deviate considerably from the reference ones. This problem turns out to be a general flaw of the embedding approach and is discussed in detail in Subsection 5.2.

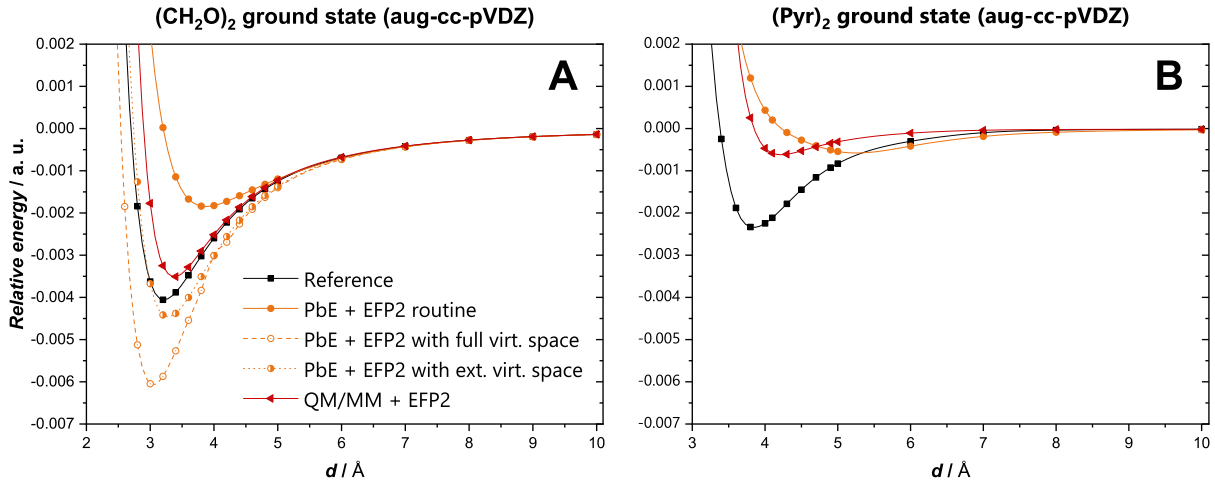

Figure 3: Relative potential energy curves of the ground states of the $(CH_2O)_2$ (Panel A) and $(Pyr)_2$ (Panel B) dimers, calculated with different models using the CCSD/aug-cc-pVDZ method as their wavefunction component.

In Figure 4 the relative potential energy curves of the ground states of the investigated complexes are shown, as calculated with cc-pVDZ basis set.

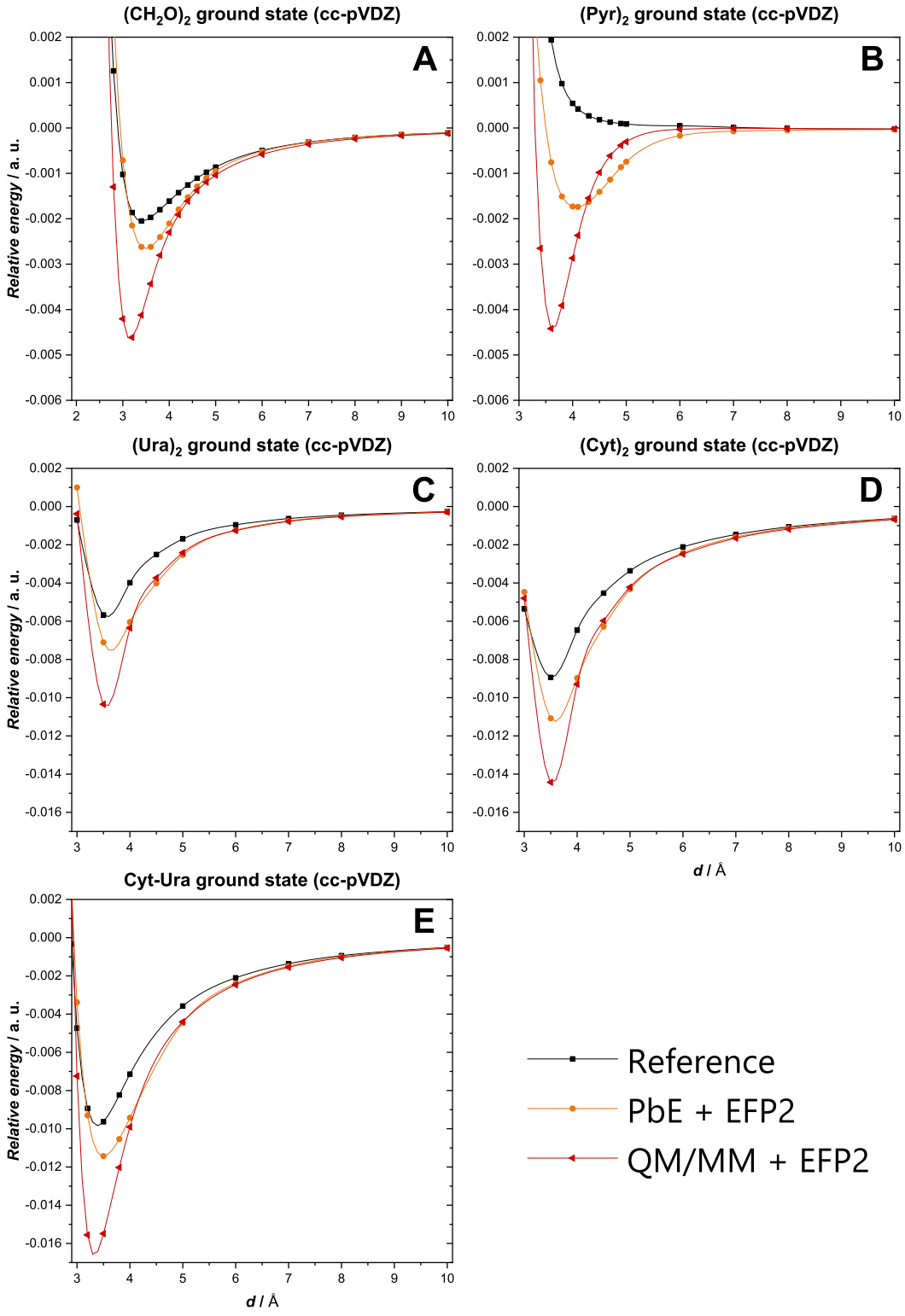

Figure 4: Relative potential energy curves of the ground states of the $(CH_2O)_2$ (Panel A), $(Pyr)_2$ (Panel B), $(Ura)_2$ (Panel C), $(Cyt)_2$ (Panel D), and *Cyt-Ura* (Panel E) complexes, calculated with different models using CCSD/cc-pVDZ method as their wavefunction component.

Figure 4 shows that both *QM/MM + EFP2* and *PbE + EFP2* overestimate the interaction energy for all systems, resulting in potential energy curves running below the reference ones. While at larger distances the two models give similar results, at shorter distances the *PbE + EFP2* curve is less bound. This indicates that the dispersion is overestimated at the EFP2/cc-pVDZ level while Pauli repulsion is better described within the PbE model than with EFP2/cc-pVDZ. Note that the ground state of $(Pyr)_2$ is not bound at the CCSD/cc-pVDZ level, thus the comparison is less relevant in that case.

5.1.2 Excited states

For homodimers it is possible to separately investigate the quality of interaction potentials without the effect of the coupling, by comparing the EFP2-corrected QM/MM and PbE curves to the average of the two reference ones. This is done here, focusing on the most important 4-10 Å range of separation. For states showing a minimum with respect to the intermolecular distance, this range covers the practically relevant parts of the attractive region.

In Figure 5 the distance dependence of various interaction potentials between two formaldehyde molecules, one in a valence excited state and the other in ground state, are plotted. The calculations were done at the CCSD/aug-cc-pVDZ level. A relatively good agreement of the *QM/MM + EFP2* curve and the averaged reference curve is observed for the $\sigma \rightarrow \pi^*$ state, suggesting that this model correctly describes the interaction and the ground state Pauli exchange and dispersion interactions are well suited for this excited state. In the $\pi - \pi^*$ state, similar agreement is observable only until 6 Å separation, below which the *QM/MM + EFP2* result deviates significantly from the reference. A closer analysis reveals a Charge Transfer (CT) state crossing the $\pi - \pi^*$ curve in this region, causing the fast descent of the reference curves (see Figure S3 in *Supplementary material*). Since the effect of CT states is not included in the fragment model at the present stage, these curves obtained with the fragment models are only reasonable above 6 Å.

The curve obtained by the *PbE + EFP2* scheme is, on the other hand, repulsive, similarly to the ground state case seen above. The reason of this failure is discussed below in more detail.

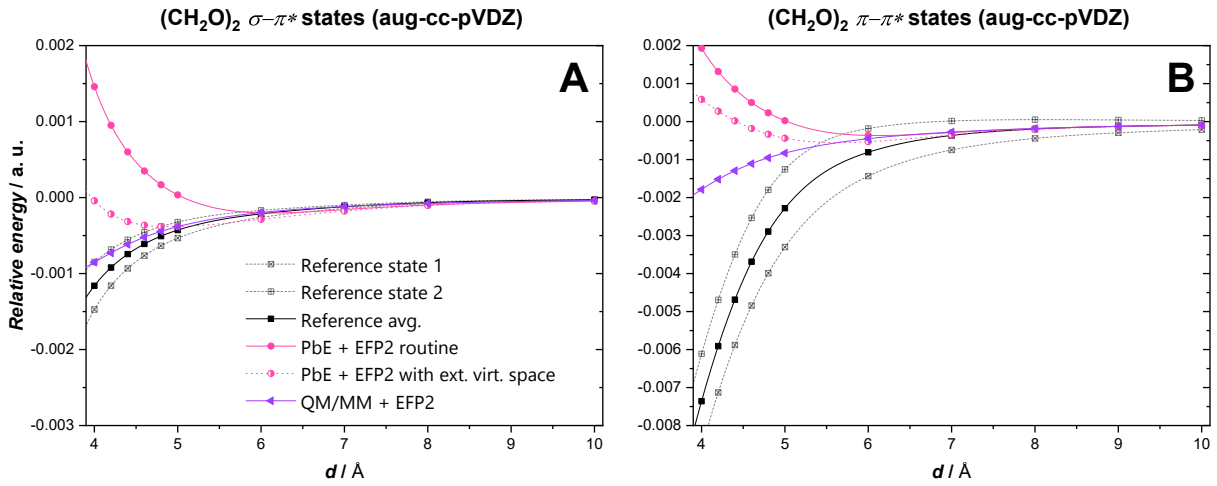

Figure 5: Distance dependence of various interaction potentials (not including interstate couplings) in the $\sigma - \pi^*$ (Panel A) and $\pi - \pi^*$ (Panel B) local valence excitations of the $(CH_2O)_2$ dimer, calculated with different models using the CCSD/aug-cc-pVDZ method as their wavefunction component.

In Figure 6 the same comparisons are shown for valence excitations of the homodimers, obtained with the cc-pVDZ basis. Now the $\pi - \pi^*$ state of $(CH_2O)_2$ can also be considered, since no interaction with CT states is present in the reference. The *QM/MM + EFP2* curves overestimate the interaction energy in all cases, just like they did in the ground state. The *PbE + EFP2* results are remarkably close to the *QM/MM + EFP2* ones, except in the case of $(Pyr)_2$ where it produces an early minimum, deviating from the attractive *QM/MM + EFP2* and reference curves.

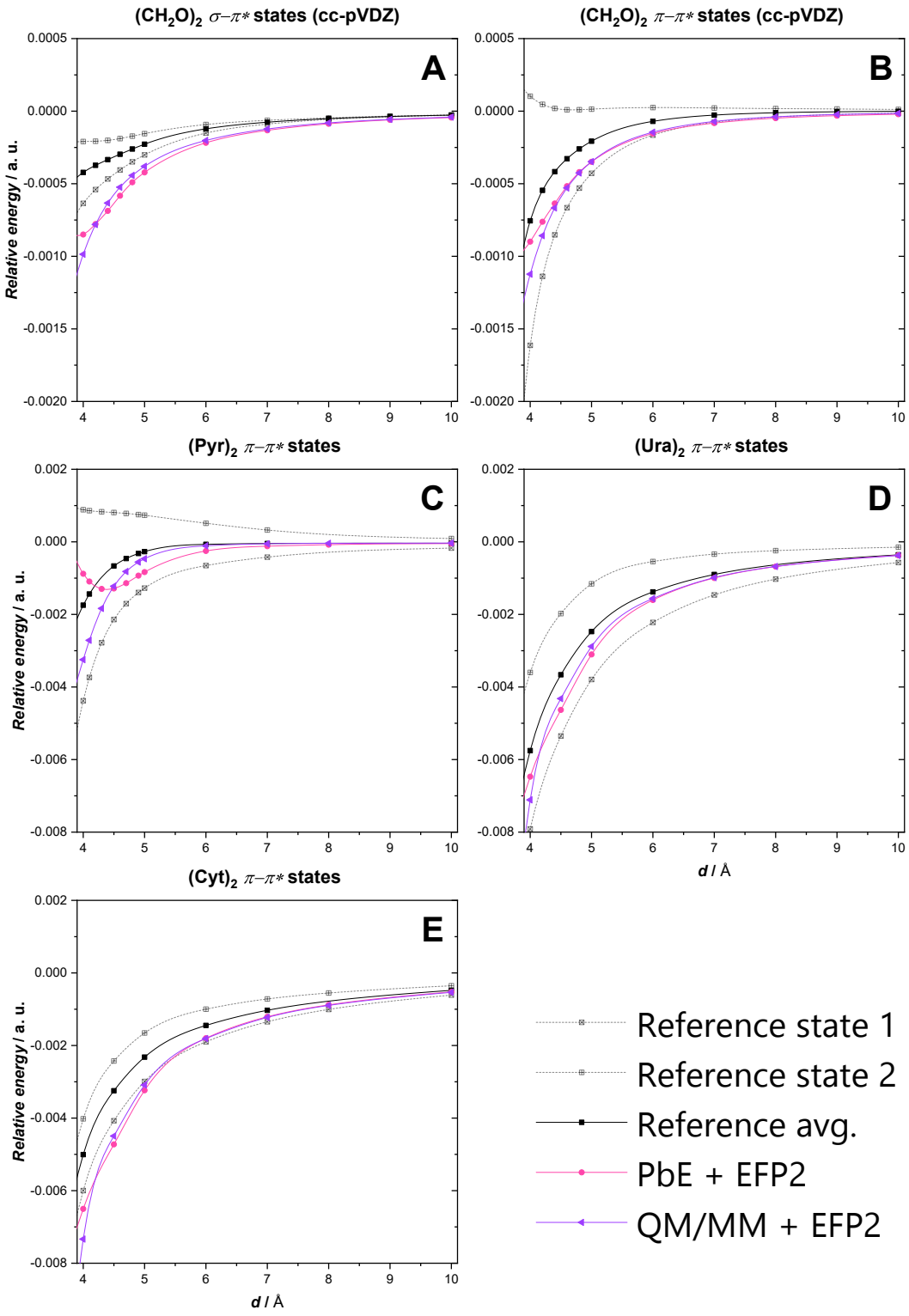

Figure 6: Distance dependence of various interaction potentials (not including interstate coupling) in valence excited states of the $(CH_2O)_2$ (Panels A and B), $(Pyr)_2$ (Panel C), $(Ura)_2$ (Panel D), and $(Cyt)_2$ (Panel E) homodimers calculated with different models using the CCSD/cc-pVDZ method as their wavefunction component.

While the present results are encouraging, one has to keep in mind that the EFP2 corrections used here were calculated with the cc-pVDZ basis set. Obviously there is no evidence that EFP2 could reproduce the interaction energy of the reference dimer calculations in this rather artificial situation. This question is, however, of moderate importance since in real applications the fragment methods should and will be used with an appropriate basis set. On the other hand, we can answer the question whether the vdW corrections obtained for the ground state represent a reasonable approximation for the case of an interacting ground state fragment and one in its excited state. To that end, we have calculated the 'exact' vdW contribution of the ground state as the energy difference of the reference ground state energy and that of the uncorrected QM/MM and PbE energies and used this quantity as an approximate vdW correction for the excited states. The corresponding curves are shown in Figure 7 for the $(Ura)_2$ and $(Cyt)_2$ systems. One finds a much better agreement with the averaged reference curve in both cases, the curves from our models running slightly above the reference ones. This means that the vdW correction from the ground state is slightly smaller than it should be in the excited state. The solid agreement of the QM/MM and PbE results indicates that it is mostly the dispersion part which is underestimated in this case.

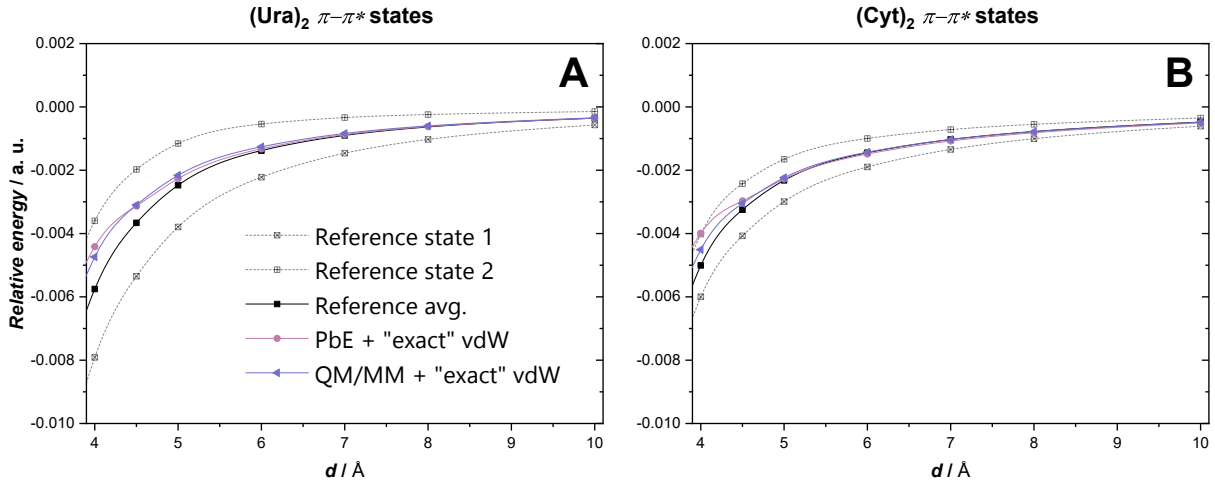

Figure 7: Distance dependence of various interaction potentials in the $\pi - \pi*$ excited states of the $(Ura)_2$ (Panel A) and $(Cyt)_2$ (Panel B) homodimers, with the vdW correction calculated from the ground state reference potential, at the CCSD/cc-pVDZ level of theory.

Continuing the investigation with the inspection of Rydberg states, in Figure 8 the distance dependence of various potentials for the Rydberg states of $(CH_2O)_2$ and $(Pyr)_2$ are

shown, obtained with the aug-cc-pVDZ basis. A striking feature one observes here is the clearly inappropriate, strongly repulsive curve produced by the by *PbE + EFP2* model (see discussion below). For *QM/MM + EFP2* the situation is much better: the curves are qualitatively correct, although the interaction energy is (except perhaps in the case of the 2nd Rydberg state pair of $(Pyr)_2$) slightly underestimated.

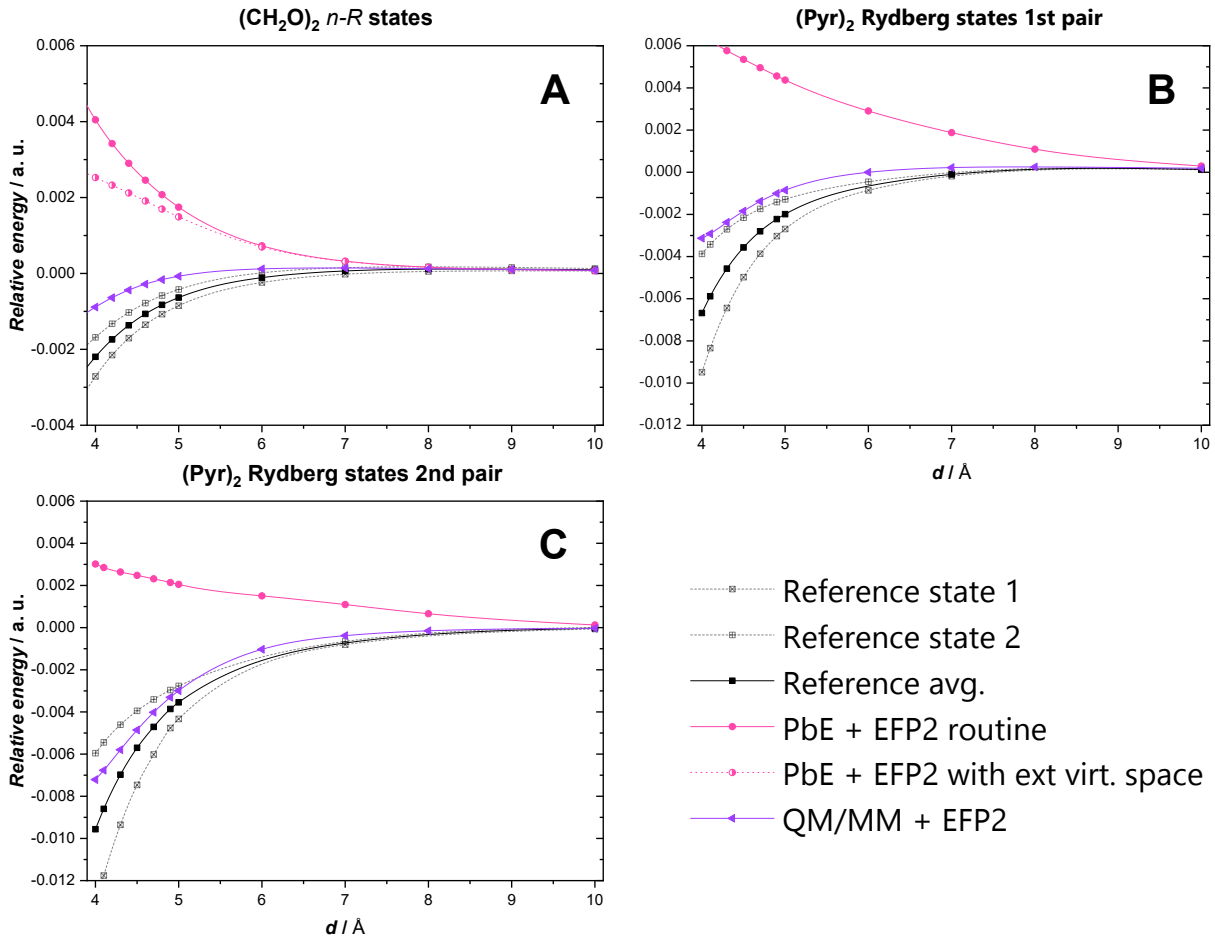

Figure 8: Distance dependence of various interaction potentials in Rydberg excited states of the $(CH_2O)_2$ (Panel A) and $(Pyr)_2$ (Panels B and C) homodimers, calculated with different models using the CCSD/aug-cc-pVDZ method as their wavefunction component.

5.2 Failure of the Huzinaga embedding scheme with diffuse basis sets

In the above discussions we have observed that the *PbE + EFP2* scheme worked well for valence excited states if used with the cc-pVDZ basis, but repulsive potential curves were

obtained with the diffuse aug-cc-pVDZ basis set. The possibility that the failure is caused by the EFP2 dispersion term can be excluded, since the same dispersion is used in *QM/MM + EFP2*, which works excellently.

On the other hand, an important feature of the present PbE scheme is the restriction of the virtual space to orbitals localized on the active fragment. As discussed earlier in Subsection 2.1.2, this step is necessary to avoid the appearance of artifactually too many charge transfer type CC excited states and to keep the cost of the correlated calculation to that of a single fragment. Unfortunately, however, this operation may seriously distort of the virtual space if diffuse functions (Rydberg orbitals) are present whose localization to the individual fragments is less obvious.

To illustrate that it is this restriction causing the problem, we have performed additional calculations on $(CH_2O)_2$ including a) all virtual orbitals of the complex (denoted as *PbE + EFP2 with full virtual space*) and b) two additional, normally excluded virtual orbitals that have the largest contribution on the active fragment (*PbE + EFP2 with extended virtual space*). The results are included in Figures 3, 5 and 8 for the ground state, for the valence excited states and for Rydberg states, respectively.

For the ground state (Figure 3), even with just two additional orbitals in the extended virtual space, the potential becomes attractive, in fact too attractive, especially if all virtual orbitals are included. Neither choice seems to be appropriate: with all orbitals included in the virtual space we see a special kind of BSSE since by decreasing the distance between the fragments, more and more virtual orbitals become available in the spatial region of the active fragment, an effect which is expected to be strong in particular with diffuse basis functions. On the other hand, restricting the virtual space to that of the active fragment causes a "reverse BSSE": by decreasing the distance, the diffuse functions of the active fragment will spatially overlap with those of the environment, causing the localization procedure to assign them to the latter. Although this effect is only visible with diffuse basis sets, it should eventually appear also with non-diffuse basis sets at very small distances.

For the valence excited states (see Figure 5) the *PbE + EFP2* curve is repulsive again, but now already with the extended virtual orbital space a minimum is observed. For the $\sigma - \pi^*$ state it is very close to the *QM/MM + EFP2* curve showing deviation only at shorter

distances. Also for the $\pi - \pi^*$ state the agreement is excellent until the the critical distance of 6Å (see above). Note that the identification of proper states with the full virtual space was not possible due to the proliferation of artificial CT states.

The concept of "reverse BSSE" is strongly supported by the fact that for Rydberg excited states the *PbE + EFP2* scheme always produces strongly repulsive potential curves (see Figure 8): here the effect is more severe since diffuse orbitals are needed to describe the dominant excitation but only orbitals spatially restricted to the active fragment are available. This effect is demonstrated on Fig. S4 in the *Supplementary material*. Note that not even the above described extension of the virtual space does solve the problem here, the curve produced by embedding with extended virtual space being still repulsive.

In summary, the present PbE scheme does not work with diffuse basis sets, and a new version is needed with proper definition of the virtual space that includes all the virtual orbitals on the active fragment, but none on the other.

5.3 Quality of the coupling schemes

The other factor that plays key role in reproducing the energy levels of interacting states is the accuracy of the coupling between local excitations, as defined in the schemes presented in Subsection 2.3. The models containing coupling terms predict a certain splitting (in the case of homodimers) or a shift (for non-symmetric complexes) of the energy levels due to the interstate interaction. To evaluate the quality of the couplings, these energy changes should be compared to those of the respective reference calculations, i.e., high-level calculations on the entire complex.

Figures 9 – 12 show the energy splittings in the symmetric complexes as functions of the intermolecular separation. For the $(CH_2O)_2$ system with aug-cc-pVDZ basis (Figure 9), a strong dependence of the results on the type of electronic state is apparent. In the $\sigma - \pi^*$ state the transition dipole approximation fails completely, predicting a practically zero splitting of the states. The TDC approach, on the other hand, gives accurate results throughout the investigated range, indicating that in this state the interaction is appropriately described by the electrostatic model if the charge distribution is considered at high resolution. For the $\pi - \pi*$ state the TDC curve is correct down to 6Å and the deviation from the reference is

still moderate around 5Å. Below this point, as discussed above, the states in the reference calculations show strong CT character, thus our model is not appropriate. In the *n-Rydberg* state the coupling is overestimated by the transition dipole approximation, while the prediction based on TDC gives correct results well down to an intermolecular distance of 4.5Å, where some deviation from the reference curve starts to show up, presumably because the contributions of the coupling that are ignored in the TDC model also become significant.

We note that the TDC results also have an obvious dependence on the electronic structure method through the accuracy of the transition density matrix predicted for the state in question. In this regard, both a close similarity as well as a significant discrepancy between the CC2 and CCSD levels could be observed, depending on the electronic state. Details are shown in Figure S2 of the *Supplementary material*.

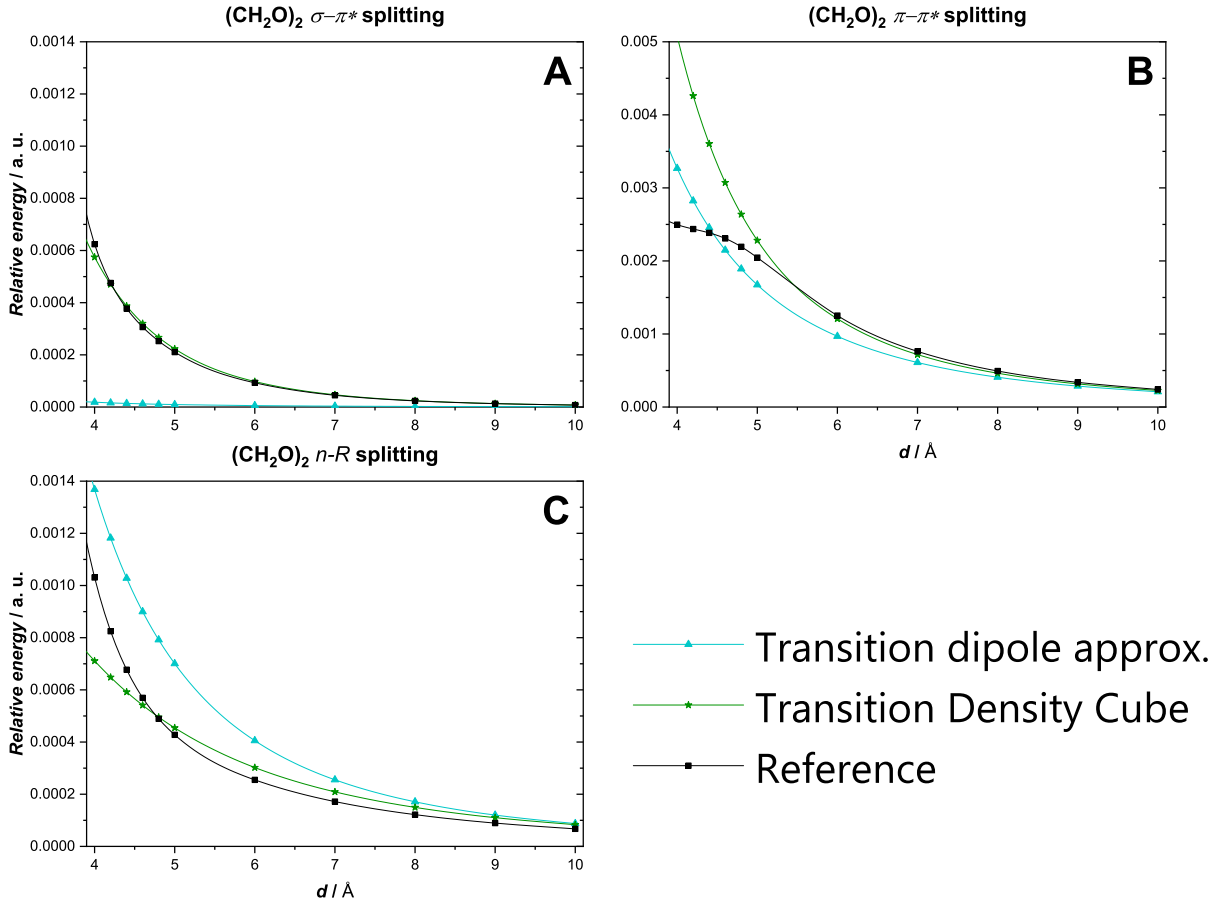

Figure 9: Dependence of the splitting (in atomic units) of the energy levels of the $(CH_2O)_2$ dimer on the intermolecular distance, as predicted by various coupling schemes.

Fig. 10 shows the couplings in the $\pi-\pi^*$ states of the *(Pyr)*$_2$, *(Cyt)*$_2$ and *(Ura)*$_2$ dimers. (Note that cc-pVDZ basis set was used for these calculations.) In these valence states, an inconsistent behavior of the transition dipole approximation is observed. While this model underestimates the coupling for *(Pyr)*$_2$ below 4.5Å, a remarkable overestimation is seen for the *(Cyt)*$_2$ and *(Ura)*$_2$ states even at larger separations. TDC, however, closely follows the reference curve in all states in the range where the Coulomb contribution dominates the coupling (about 5 Å for *(Pyr)*$_2$, 4 Å for *(Cyt)*$_2$ and 3.5 Å for *(Ura)*$_2$). Below these points, it starts to deviate from the reference, indicating the importance of the missing exchange (Dexter) contributions to the splitting. Since for the latter two systems these points are comfortably close to the ground state equilibrium separation, it can be inferred that the TDC model provides a reliable prediction of the splitting in the entire attractive side of the interacting PES.

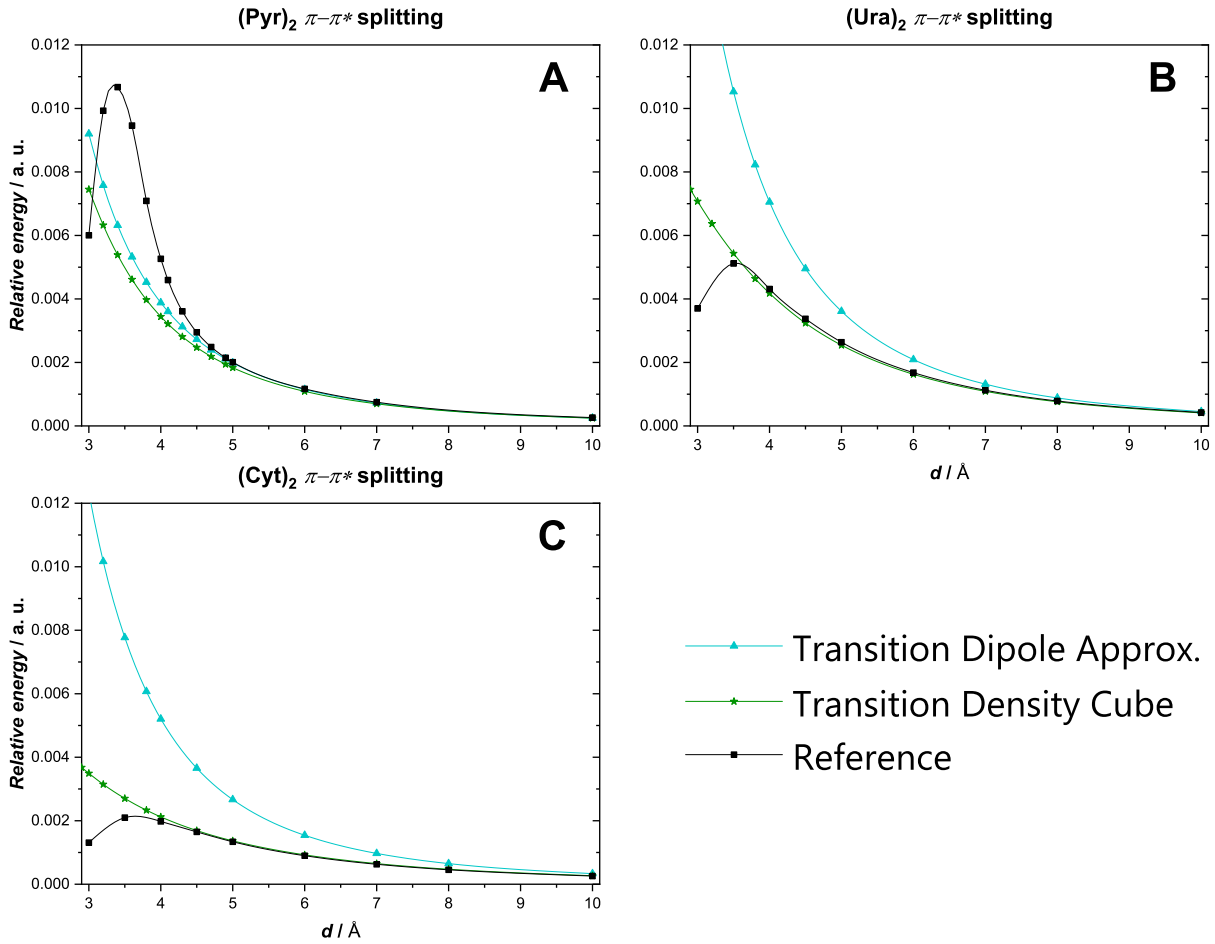

Figure 10: Dependence of the splitting (in atomic units) of the $\pi - \pi*$ energy levels of the *(Pyr)*$_2$ (panel A), *(Cyt)*$_2$ (panel B) and *(Ura)*$_2$ (panel C) dimers on the intermolecular distance, as predicted by various coupling schemes.

The energy splitting of the corresponding states in the asymmetric *Cyt-Ura* complex is shown on Fig. 11. Since in this case the energy gap is nonzero even at infinite separation, the splitting is defined here as

$$\Delta E_{split}(R) := \Delta E(R) - \Delta E(\infty), \tag{22}$$

for all methods.

The change of the gaps with the distance is much smaller in this complex than in either the *(Cyt)*$_2$ or the *(Ura)*$_2$ systems. TrDA shows a behavior similar to the above cases, severely overestimating the growth of the energy gap with the fragments approaching each

other. The TDC model, on the other hand, shows a good agreement with the reference, with only a moderate underestimation of the splitting below 5Å.

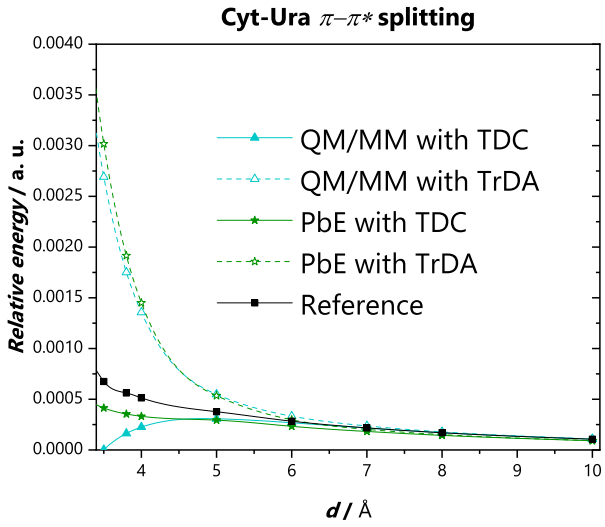

Figure 11: Dependence of the difference (in atomic units) of the $\pi - \pi^*$ energy levels in the *Cyt-Ura* complex on the intermolecular distance, as predicted by various coupling schemes. The reference curve is defined relative to the energy gap at infinite separation.

A very different picture is seen for the 1st and 2nd pairs of Rydberg states of the $(Pyr)_2$ dimer on Fig. 12. (Note that, obviously, the diffuse basis aug-cc-pVDZ was used here.) TrDA completely fails for the 1st pair, predicting a zero coupling between these dark excited states. The refined evaluation of the Coulombic coupling by the TDC model provides a reasonable result for the first pair of states until 6 Å, but severely underestimates the reference curve at smaller separations, indicating the necessity of the exchange (Dexter) terms for a reasonable prediction of the coupling. The monomer state of the 2nd Rydberg pair possesses a non-zero transition dipole moment, hence the splitting could in principle be approximated from this scheme. However, it is larger than its TDC counterpart, similarly to the n-R excitation of $(CH_2O)_2$ discussed above. This insinuates the conclusion that for these type of states TrDA overestimates the Coulombic (Frenkel) coupling between the two monomers. The resulting splitting is, however, still much smaller than that of the reference curves, showing that the overestimation is far from canceling the error from the absence of the Dexter terms in our methods. These findings make it clear that both models investigated here are inappropriate for modeling couplings between Rydberg type excited states.

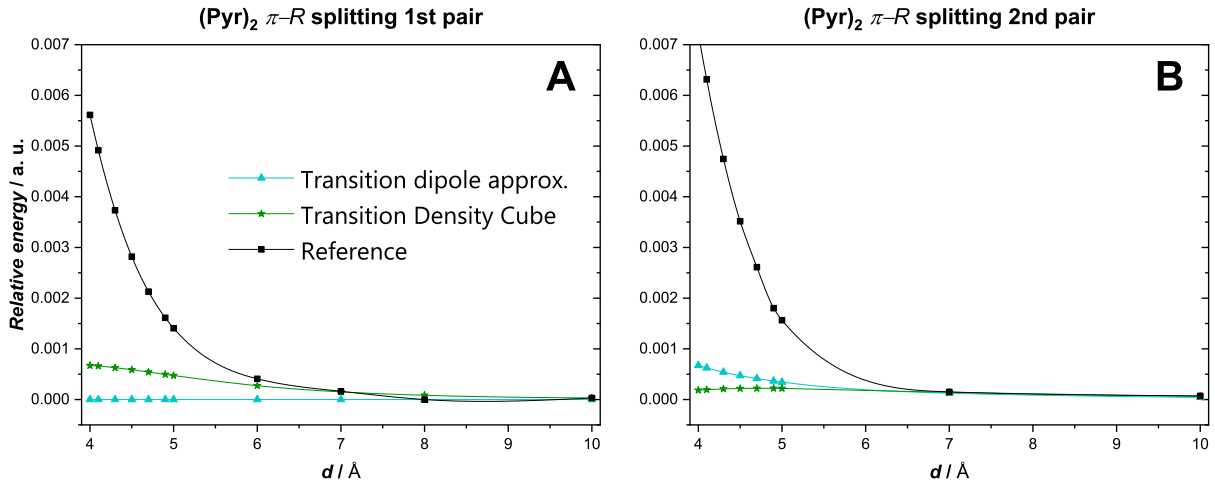

Figure 12: Distance dependence of the splitting (in atomic units) of the first (Panel A) and second (Panel B) pair of Rydberg energy levels in the *(Pyr)*$_2$ complex, as predicted by various coupling schemes at the CCSD / aug-cc-pVDZ level of theory.

5.4 Potential energy curves

The different interaction energy and interstate coupling models result in a variety of final predictions for excited state potential energy curves. Since the evaluation of the coupling terms in Section 5.3 demonstrated the clear superiority of the TDC scheme over the one based solely on transition dipoles, surfaces resulting from the combination of TDC couplings (calculated at the CCSD level of theory) and various interaction energy potentials will be discussed in this chapter to assess the final results. As in Section 5.1, the 4 - 10 Å range of intermolecular separation is investigated.

5.4.1 Valence excited states

The potential energy surfaces, relative to the sum of the respective monomer electronic energies, are shown for the valence type electronic states in Figs. 13 and 14. For *(*CH_2O*)*$_2$ results obtained with the aug-cc-pVDZ basis set are shown (Figure 13), while for the larger complexes (Figure 14) the cc-pVDZ basis set was used.

In the $\sigma - \pi^*$ state of *(*CH_2O*)*$_2$ the *QM/MM + EFP2* model is generally well suited to describe the PES of both states in the whole investigated range, with the same accuracy. Severe discrepancies are seen for the *PbE + EFP2* scheme, however: both states turn strongly

repulsive at as early as 6Å separation. This behavior stems from the incorrect virtual orbital selection as described earlier in Section 5.2.

The $\pi - \pi^*$ state of the formaldehyde dimer is, as discussed in Section 5.1.2 strongly influenced by a crossing CT state below 6 Å if diffuse functions are present in the basis set. Since the models do not include charge transfer effects, neither method can be expected to produce a satisfactory result at short separations. This is, as seen on Figure 13, indeed the case, the surfaces obtained from the *PbE + EFP2* model being so overly repulsive that only the lower one features a shallow intermolecular minimum around 5Å, while the upper one exhibits a strong, obviously incorrect repulsive character. *QM/MM + EFP2* also underestimates the attraction in both states, as seen already on the coupling-free surfaces of Figure 5. On the other hand, anywhere above 6 Å, both models agree well with the reference. From the two the *QM/MM + EFP2* results are to some degree more accurate, but the difference is insignificant. This suggests that without the interacting CT states complicating the wavefunctions, both approaches could produce meaningful potential energy surfaces even at shorter distances.

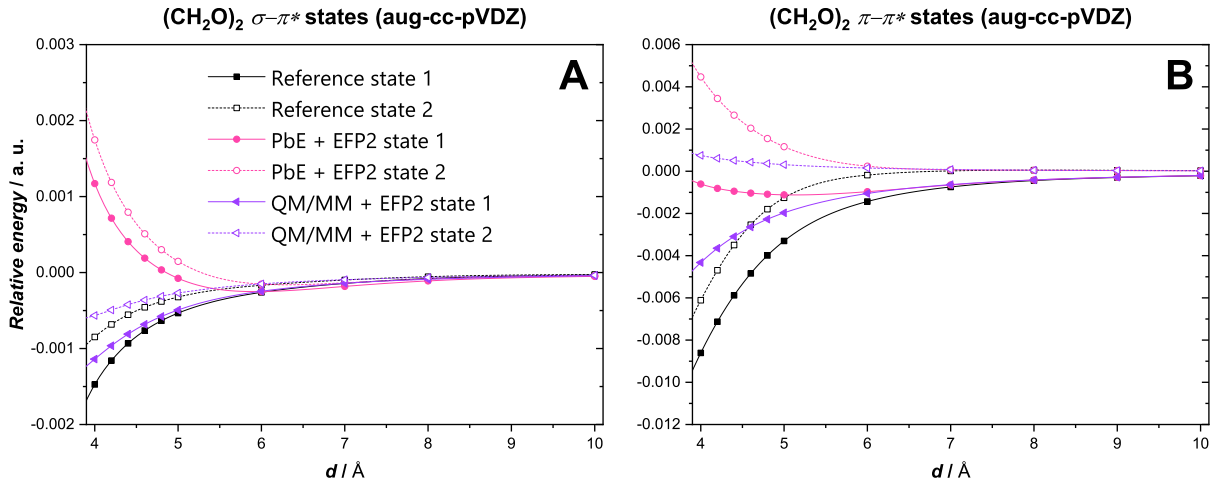

Figure 13: Potential energy curves (relative to the values at infinite separation, in atomic units) of the investigated $\sigma - \pi^*$ (Panel A) and $\pi - \pi^*$ (Panel B) valence excited states of the $(CH_2O)_2$ complex, calculated at with different models using CCSD/aug-cc-pVDZ method as their wavefunction component.

The effect of other states is mostly eliminated if no diffuse functions are present in the basis set, as seen on Figure 14. In the investigated $\pi - \pi^*$ state pair of $(Pyr)_2$ (Panel A) both

the *PbE + EFP2* and the *QM/MM + EFP2* models produce a nearly perfect agreement with the reference until 6 Å. Below this point, the *PbE + EFP2* potential energies start to become somewhat too low and show an unphysical minimum between 4 and 6 Å . This turn-back is likely caused by the truncation of the virtual orbital space in the PbE excitation energy calculations, artificially eliminating certain excitations of the dimer wavefunction. The *QM/MM + EFP2* results are, in principle, correct until 5 Å, where both curves start to run under the reference. While the error still remains moderate for the rapidly decreasing lower state, the upper one is significantly overstabilized and fails to reproduce the repulsive nature of the reference surface.

The approximate models are generally well suited for the $(Ura)_2$ and $(Cyt)_2$ $\pi - \pi^*$ dimer states (Panels B and C of Fig. 14). The shape of the potential energy curves follow those of the reference, with a modest underestimation by both methods. The *QM/MM + EFP2* approach turns out slightly more accurate until 4.5 Å, but the difference to the embedding results is negligible anywhere over 5 Å. The deviation from the reference is more significant in the $(Cyt)_2$ case, both in relative and nominal terms. Based on the findings discussed in Section 5.3 it is clear that the discrepancy is mostly caused by the error of the interaction energy modeling, as the interstate couplings are almost perfectly reproduced in the investigated region.

The potential energies of the same electronic states of the *Cyt-Ura* complex are shown in Panel D of Figure 14. (Note that the zero point of the energy scale is defined as the mean of the dimer excited state energies at infinite separation.) Here the *PbE + EFP2* potentials are in good agreement with the reference in the entire region. The *QM/MM + EFP2* result is also correct, almost indistinguishable from the *PbE + EFP2* one above 4.5 Å, while a somewhat stronger underestimation of the reference energies is produced below this point. Generally, the relative agreement with the reference is better in this non-symmetric complex than expected from the results on the homodimers $(Cyt)_2$ and $(Ura)_2$. This accentuates the complexity of the excited state interactions in stacked π-complexes.

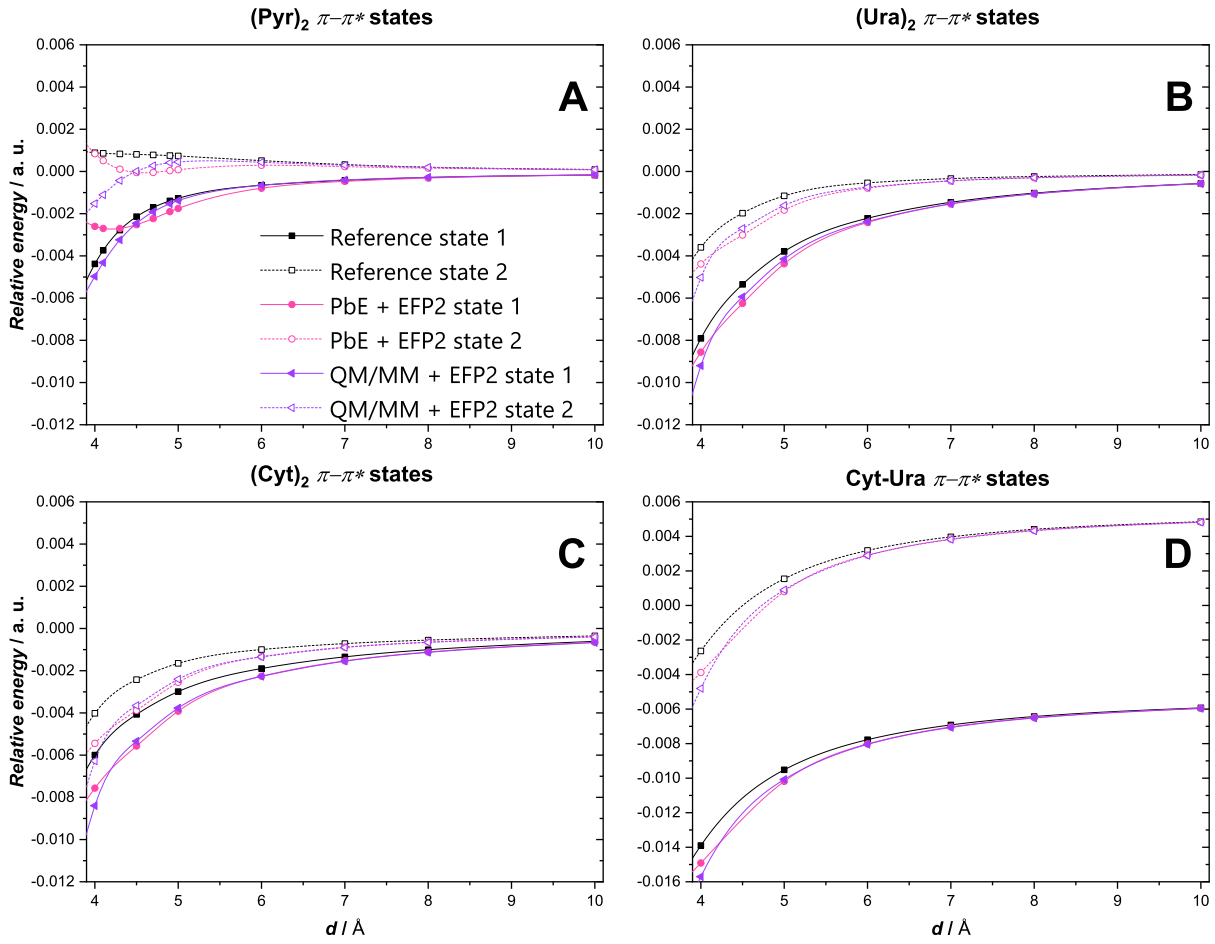

Figure 14: Potential energy curves (relative to the mean total energies at infinite separation, in atomic units) of the investigated $\pi - \pi^*$ excited states in the *(Pyr)*$_2$ (Panel A), *(Cyt)*$_2$ (Panel B), *(Ura)*$_2$ (Panel C) and *Cyt-Ura* (Panel D) complexes, calculated with different models using CCSD/cc-pVDZ method as their wavefunction component.

5.4.2 Rydberg states

Rydberg type electronic states, as seen above in Sections 5.1.2 and 5.3, represent a big challenge for the interaction modeling. The potential energy curves, shown on Fig. 15 for *(Pyr)*$_2$ and the *(CH*$_2$*O)*$_2$, reflect many features already seen on the interaction energies above. The *PbE + EFP2* model produces nonphysical, repulsive surfaces for both interacting states in all cases. This makes it clear that this approach in its present form is not suited for Rydberg type excited states. The *QM/MM + EFP2* energies, on the other hand, follow the reference with good parallelism in the whole range. However, due to the improper prediction of the coupling for Rydberg states (see Section 5.3), the splitting of the states is severely

underestimated. The resulting surfaces are thus also incorrect from the very point where the interaction becomes significant - as early as 6Å separation in these cases. This clearly indicates that for a qualitatively correct recovery of the Rydberg surfaces in the *QM/MM + EFP2* framework, the appropriate modeling of the coupling is also indispensable.

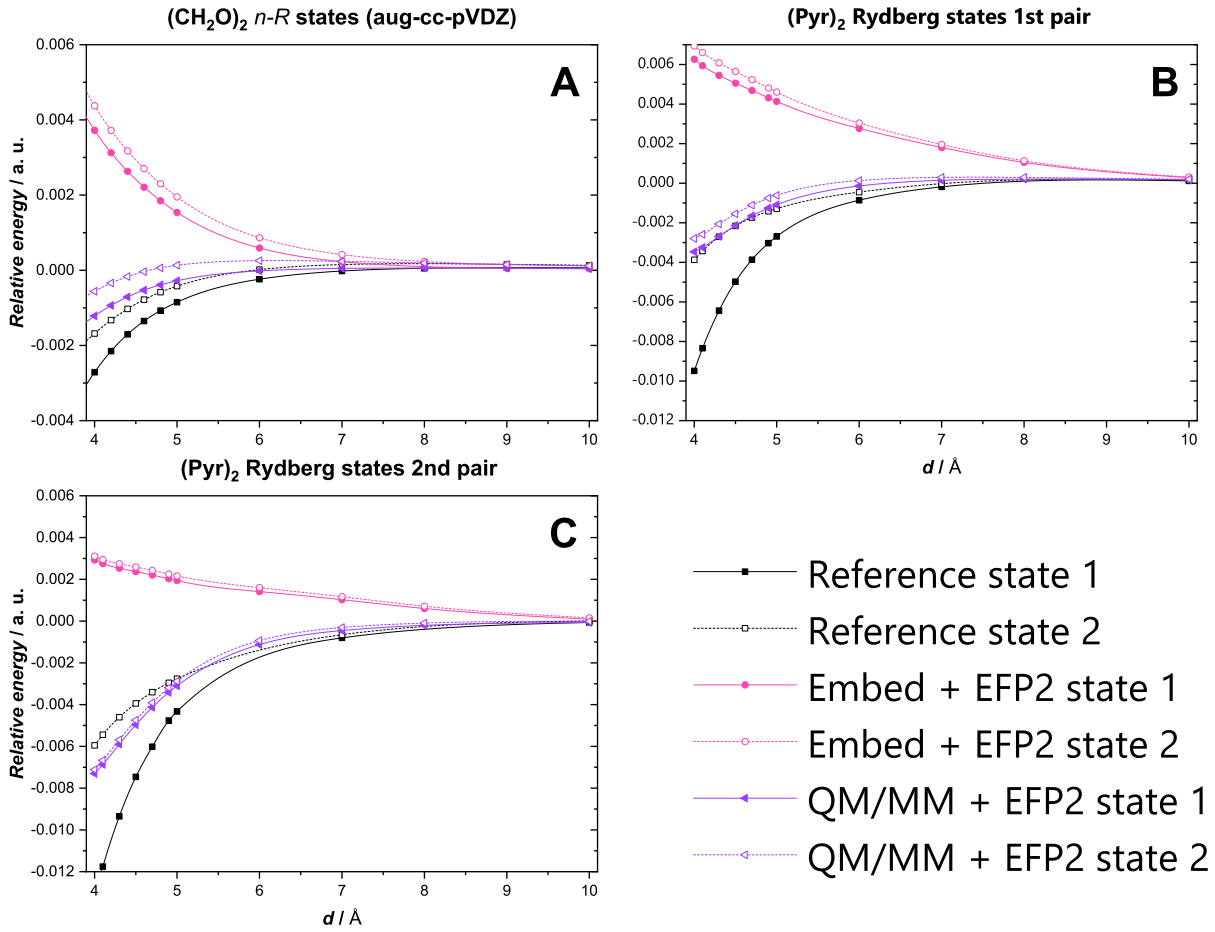

Figure 15: Potential energy curves (relative to the values at infinite separation, in atomic units) of the investigated Rydberg excited states in the $(CH_2O)_2$ (Panel A) and $(Pyr)_2$ (Panels B and D) dimers, evaluated with different models using CCSD/aug-cc-pVDZ method as their wavefunction component.

6 Conclusions

For the theoretical description of non-covalent interactions in excited states, various fragment-based methods have been formulated and tested on stacked complexes of formaldehyde, pyrrole, uracil, and cytosine.

Regarding the electronic structure calculations on the fragments, both the QM/MM model (with CHELPG point charges representing the environment), and the projector-based embedding approach (PbE) were found to be good choices, as long as no diffuse functions are present in the basis set. With diffuse basis functions included, QM/MM performs similarly, but a PbE model fails due to the use of a localized and truncated virtual space that results in incorrectly repulsive potential energy curves.

Achieving satisfactory accuracy for the potential energy curves requires that the van der Waals-type interactions (dispersion and Pauli repulsion) are also properly included. The examples presented in this work confirm that the respective EFP2 terms obtained for the ground state provide a convenient and accurate approximation for these interactions between a ground state and an excited state fragment.

An appropriate consideration of the Frenkel splitting is also necessary to model interacting states; it was found that the relatively simple TDC scheme is able to predict the Coulomb part of the associated excitonic coupling at a high accuracy. Neglect of the Dexter part of the coupling was noticeable only at small intermolecular separations (below 4 Å in the complexes investigated here).

The proposed methodology produces reasonably accurate potential energy curves above separation of 4 Å. This is essentially the range from the intermolecular energy minima (when the electronic state exhibits one) up to dissociation, thus representing the regime relevant for phenomena related to complex formation and stability.

Despite the encouraging results presented here, we see several points where the suggested methodologies could be improved. First, the PbE scheme needs to be made suitable for calculations with diffuse basis sets. To this end, a new localization scheme for the virtual orbitals is apparently needed. Second, we believe that the development of state-specific dispersion and Pauli repulsion terms could improve the reliability of the interaction energy. Note that similar developments are needed for TD-DFT methods to include state-specific dispersion interaction.[62] Third, to also reliably predict equilibrium structures of these complexes, the inclusion of the Dexter coupling is necessary. At present, the highest-level wavefunction method available for this purpose is CC2,[66] but our results (discussed in the *Supplementary material* of this paper) show that the transition properties predicted by this method can be

very different from those obtained with CCSD (see also Ref. 103). Finally, the interaction between valence and charge transfer states needs to be included in this scheme, which could be done by means of the adaptation of the TD-DFT procedure suggested by Li *et al.*[71]

Significant effort has also been put into producing CCSD-level benchmark data for a reliable test of the fragment methods. The associated difficulties (e.g correction for BSSE of excited states) have also been discussed. These data can later be used in benchmarking cheaper supermolecular methods, similarly to a recent study by Hancock and Goerigk[62] on different TD-DFT methods. The data are provided in Tables S10-12 of the *Supplementary material*.

Acknowledgments

This work has been supported by the National Research, Innovation and Development Fund (NKFIA) of Hungary Grant No. 124018. We thank Prof. Mihály Kállay and his coworkers for assisting the embedding calculations and making adjustments in the MRCC code. JFS acknowledges for Fulbright fellowship. The authors thank Prof. Géza Fogarasi for his help finalizing the manuscript.

Data availability statement

The data supporting the findings of this study are available in the supplementary material.

Conflict of interest

The authors declare no conflict of interest.

Supporting Information

Structures of the monomers and complexes evaluated in this study, the impact of "exact" ground state van-der-Waals terms on the homodimer excited state surfaces, comparison of

the CCSD and CC2 excited state splittings in the $(CH_2O)_2$ system, excited state total energy curves of $(CH_2O)_2$ as well as the reference CCSD data for all studied states are presented here. In addition, the failure of the localization of virtual orbitals are demonstrated by showing a Rydberg orbital obtained in the PbE procedure at different intermolecular distances. Details of the calculation of the CHelpG charges and their values used in this study are also given.

References

1. González, L.; Escudero, D.; Serrano-Andrés, L. Progress and Challenges in the Calculation of Electronic Excited States. *ChemPhysChem* **2012**, *13*, 28–51.

2. Tajti, A.; Szalay, P. G. Investigation of the Impact of Different Terms in the Second Order Hamiltonian on Excitation Energies of Valence and Rydberg States. *J. Chem. Theory Comput.* **2016**, *12*, 5477–5482.

3. Crawford, T. D.; Kumar, A.; Bazanté, A. P.; Di Remigio, R. Reduced-scaling coupled cluster response theory: Challenges and opportunities. *WIREs Computational Molecular Science* **2019**, *9*, e1406.

4. Izsák, R. Single-reference coupled cluster methods for computing excitation energies in large molecules: The efficiency and accuracy of approximations. *WIREs Computational Molecular Science* **2020**, *10*, e1445.

5. Tajti, A.; Kozma, B.; Szalay, P. G. Improved Description of Charge-Transfer Potential Energy Surfaces via Spin-Component-Scaled CC2 and ADC(2) Methods. *J. Chem. Theory Comput.* **2021**, *17*, 439–449, PMID: 33326229.

6. Senn, H. M.; Thiel, W. QM/MM Methods for Biomolecular Systems. *Angew Chem Int Edit* **2009**, *48*, 1198–1229.

7. Chung, L. W.; Sameera, W. M. C.; Ramozzi, R.; Page, A. J.; Hatanaka, M.; Petrova, G. P.; Harris, T. V.; Li, X.; Ke, Z.; Liu, F.; Li, H.-B.; Ding, L.; Morokuma, K. The ONIOM Method and Its Applications. *Chemical Reviews* **2015**, *115*, 5678–5796.

8. Manby, F. R.; Stella, M.; Goodpaster, J. D.; Miller, T. F. I. A Simple, Exact Density-Functional-Theory Embedding Scheme. *Journal of Chemical Theory and Computation* **2012**, *8*, 2564–2568, PMID: 22904692.

9. Wesolowski, T. A.; Warshel, A. Frozen density functional approach for ab initio calculations of solvated molecules. *The Journal of Physical Chemistry* **1993**, *97*, 8050–8053.

10. Wesołowski, T. A. Embedding a multideterminantal wave function in an orbital-free environment. *Physical Review A* **2008**, *77*, 012504.

11. Crawford, T. D.; King, R. A. Locally correlated equation-of-motion coupled cluster theory for the excited states of large molecules. *Chem. Phys. Lett.* **2002**, *366*, 611.

12. Korona, T.; Werner, H.-J. Local treatment of electron excitations in the EOM-CCSD method. *J. Chem. Phys.* **2003**, *118*, 3006.

13. Kats, D.; Korona, T.; Schütz, M. Local CC2 electronic excitation energies for large molecules with density fitting. *J. Chem. Phys.* **2006**, *125*, 104106.

14. Ma, Q.; Werner, H.-J. Explicitly correlated local coupled-cluster methods using pair natural orbitals. *Wiley Interdiscip. Rev.: Comput. Mol. Sci.* **2018**, *8*, e1371.

15. Dutta, A. K.; Saitow, M.; Riplinger, C.; Neese, F.; Izsák, R. A nearlinear scaling equation of motion coupled cluster method for ionized states. *J. Chem. Phys.* **2018**, *148*, 244101.

16. Mester, D.; Nagy, P. R.; Kállay, M. Reduced-cost second-order algebraic-diagrammatic construction method for excitation energies and transition moments. *J. Chem. Phys.* **2018**, *148*, 094111.

17. Mester, D.; Nagy, P. R.; Kállay, M. Reduced-scaling correlation methods for the excited states of large molecules: Implementation and benchmarks for the second-order algebraic-diagrammatic construction approach. *J. Chem. Theory Comput.* **2019**, *15*, 6111.

18. Benda, Z.; Szalay, P. G. Characterization of the Excited States of DNA Building Blocks: a Coupled Cluster Computational Study. *Phys. Chem. Chem. Phys.* **2016**, *18*, 23596–23606.

19. Gordon, M. S.; Fedorov, D. G.; Pruitt, S. R.; Slipchenko, L. V. Fragmentation Methods: A Route to Accurate Calculations on Large Systems. *Chem. Rev.* **2011**, *112*, 632–672.

20. Szalay, P. G.; Watson Jr., T. J.; Perera, A.; Lotrich, V. F.; Fogarasi, G.; Bartlett, R. J. Benchmark Studies on the Building Blocks of DNA: 2. Effect of Biological Environment on the Electronic Excitation Spectrum of Nucleobases. **2012**, *116*, 8851–8860.

21. Barcza, B.; Szirmai, Á. B.; Szántó, K. J.; Tajti, A.; Szalay, P. G. Comparison of approximate intermolecular potentials for ab initio fragment calculations on medium sized N-heterocycles. *Journal of Computational Chemistry* **2022**, *43*, 1079–1093.

22. Gordon, M. S.; Slipchenko, L.; Li, H.; Jensen, J. H. In *Chapter 10 The Effective Fragment Potential: A General Method for Predicting Intermolecular Interactions*; Spellmeyer, D., Wheeler, R., Eds.; Annual Reports in Computational Chemistry; Elsevier, 2007; Vol. 3; pp 177–193.

23. Stone, A. J. Distributed Multipole Analysis: Stability for Large Basis Sets. *Journal of Chemical Theory and Computation* **2005**, *1*, 1128–1132, PMID: 26631656.

24. Jensen, J. H.; Gordon, M. S. An approximate formula for the intermolecular Pauli repulsion between closed shell molecules. II. Application to the effective fragment potential method. *The Journal of Chemical Physics* **1998**, *108*, 4772–4782.

25. Frenkel, J. A. On the transformation of light into heat in solids. II. *Phys. Rev.* **1931**, *37*, 1276.

26. Davydov, A. S. *Soviet Phys.-Usp* **1964**, *530*, 145–180.

27. Morrison, A. F.; You, Z. Q.; Herbert, J. M. Ab initio implementation of the Frenkel–Davydov exciton model: a naturally parallelizable approach to computing collective excitations in crystals and aggregates. *Journal of Chemical Theory and Computation* **2014**, *10*, 5366 – 5376.

28. Sisto, A.; Stross, C.; van der Kamp, M. W.; O'Connor, M.; McIntosh-Smith, S.; Johnson, G. T.; Hohenstein, E. G.; Manby, F. R.; Glowacki, D. R.; Martinez, T. J. Atomistic non-adiabatic dynamics of the LH2 complex with a GPU-accelerated ab initio exciton model. *Phys. Chem. Chem. Phys.* **2017**, *19*, 14924–14936.

29. Amadei, A.; D'Alessandro, M.; D'Abramo, M.; Aschi, M. Theoretical characterization of electronic states in interacting chemical systems. *The Journal of Chemical Physics* **2009**, *130*, 084109.

30. Hégely, B.; Szirmai, Á. B.; Mester, D.; Tajti, A.; Szalay, P. G.; Kállay, M. Performance of Multilevel Methods for Excited States. *The Journal of Physical Chemistry A* **2022**, *126*, 6548–6557, PMID: 36095318.

31. Ge, Q.; Head-Gordon, M. Energy decomposition analysis for excimers using absolutely localized molecular orbitals within time-dependent density functional theory and configuration interaction .... *Journal of Chemical Theory and Computation* **2018**, *14*, 5156–5168.

32. Ponder, J. W.; Case, D. A. *Protein Simulations*; Advances in Protein Chemistry; Academic Press: San Diego, CA, 2003; Vol. 66; pp 27–85.

33. Wang, J.; Wolf, R. M.; Caldwell, J. W.; Kollman, P. A.; Case, D. A. Development and testing of a general amber force field. *Journal of Computational Chemistry* **2004**, *25*, 1157–1174.

34. Brooks, B. R.; Brooks III, C. L.; Mackerell Jr., A. D.; Nilsson, L.; Petrella, R. J.; Roux, B.; Won, Y.; Archontis, G.; Bartels, C.; Boresch, S.; Caflisch, A.; Caves, L.; Cui, Q.; Dinner, A. R.; Feig, M.; Fischer, S.; Gao, J.; Hodoscek, M.; Im, W.; Kuczera, K.; Lazaridis, T.; Ma, J.; Ovchinnikov, V.; Paci, E.; Pastor, R. W.; Post, C. B.; Pu, J. Z.; Schaefer, M.; Tidor, B.; Venable, R. M.; Woodcock, H. L.; Wu, X.; Yang, W.; York, D. M.; Karplus, M. CHARMM: The biomolecular simulation program. *Journal of Computational Chemistry* **2009**, *30*, 1545–1614.

35. Stone, A. Distributed multipole analysis, or how to describe a molecular charge distribution. *Chemical Physics Letters* **1981**, *83*, 233–239.

36. Stone, A. J. *The Theory of Intermolecular Forces*; OUP Oxford: Oxford, 2013.

37. Day, P. N.; Jensen, J. H.; Gordon, M. S.; Webb, S. P.; Stevens, W. J.; Krauss, M.; Garmer, D.; Basch, H.; Cohen, D. An effective fragment method for modeling solvent

effects in quantum mechanical calculations. *The Journal of Chemical Physics* **1996**, *105*, 1968–1986.

38. Gordon, M. S.; Smith, Q. A.; Xu, P.; Slipchenko, L. V. Accurate First Principles Model Potentials for Intermolecular Interactions. *Annual Review of Physical Chemistry* **2013**, *64*, 553–578.

39. Sattasathuchana, T.; Xu, P.; Gordon, M. S. An Accurate Quantum-Based Approach to Explicit Solvent Effects: Interfacing the General Effective Fragment Potential Method with Ab Initio Electronic Structure Theory. *The Journal of Physical Chemistry A* **2019**, *123*, 8460–8475.

40. Breneman, C. M.; Wiberg, K. B. Determining atom-centered monopoles from molecular electrostatic potentials. The need for high sampling density in formamide conformational analysis. *Journal of Computational Chemistry* **1990**, *11*, 361–373.

41. Huzinaga, S.; Cantu, A. A. Theory of Separability of Many-Electron Systems. *The Journal of Chemical Physics* **1971**, *55*, 5543–5549.

42. Hégely, B.; Nagy, P. R.; Ferenczy, G. G.; Kállay, M. Exact density functional and wave function embedding schemes based on orbital localization. *The Journal of Chemical Physics* **2016**, *145*, 064107.

43. Khait, Y. G.; Hoffmann, M. R. In *Annual Reports in Computational Chemistry*; Wheeler, R. A., Ed.; Annual Reports in Computational Chemistry; Elsevier, 2012; Vol. 8; pp 53–70.

44. Bennie, S. J.; Curchod, B. F. E.; Manby, F. R.; Glowacki, D. R. Pushing the Limits of EOM-CCSD with Projector-Based Embedding for Excitation Energies. *The Journal of Physical Chemistry Letters* **2017**, *8*, 5559–5565, PMID: 29076727.

45. Parravicini, V.; Jagau, T.-C. Embedded equation-of-motion coupled-cluster theory for electronic excitation, ionisation, electron attachment, and electronic resonances. *Molecular Physics* **2021**, *119*, e1943029.

46. Claudino, D.; Mayhall, N. J. Simple and Efficient Truncation of Virtual Spaces in Embedded Wave Functions via Concentric Localization. *The Journal Chemical Theory and Computations* **2019**, *15*, 6085 – 6096.

47. Hégely, B.; Szirmai, Á. B.; Mester, D.; Tajti, A.; Szalay, P. G.; Kállay, M. Performance of Multilevel Methods for Excited States. *The Journal of Physical Chemistry A* **2022**, *126*, 6548–6557, PMID: 36095318.

48. Claudino, D.; Mayhall, N. J. Automatic Partition of Orbital Spaces Based on Singular Value Decomposition in the Context of Embedding Theories. *Journal of Chemical Theory and Computation* **2019**, *15*, 1053–1064.

49. Jensen, J. H.; Gordon, M. S. An approximate formula for the intermolecular Pauli repulsion between closed shell molecules. *Molecular Physics* **1996**, *89*, 1313–1325.

50. Jensen, J. H. Intermolecular exchange-induction and charge transfer: Derivation of approximate formulas using nonorthogonal localized molecular orbitals. *The Journal of Chemical Physics* **2001**, *114*, 8775–8783.

51. Adamovic, I.; *, M. S. G. Dynamic polarizability, dispersion coefficient C6 and dispersion energy in the effective fragment potential method. *Molecular Physics* **2005**, *103*, 379–387.

52. Smith, Q. A.; Ruedenberg, K.; Gordon, M. S.; Slipchenko, L. V. The dispersion interaction between quantum mechanics and effective fragment potential molecules. *The Journal of Chemical Physics* **2012**, *136*, 244107.

53. Smith, T.; Slipchenko, L. V.; Gordon*, M. S. Modeling $\pi - \pi$ Interactions with the Effective Fragment Potential Method: The Benzene Dimer and Substituents. *The Journal of Physical Chemistry A* **2008**, *112*, 5286–5294, PMID: 18476681.

54. Sattasathuchana, T.; Xu, P.; Gordon, M. S. An Accurate Quantum-Based Approach to Explicit Solvent Effects: Interfacing the General Effective Fragment Potential Method with Ab Initio Electronic Structure Theory. *The Journal of Physical Chemistry A* **2019**, *123*, 8460–8475, PMID: 31365250.

55. Rojas, C. I. V.; Slipchenko, L. V. Exchange Repulsion in Quantum Mechanical/Effective Fragment Potential Excitation Energies: Beyond Polarizable Embedding. *Journal of Physical Chemistry Letters* **2020**, *16*, 6408 – 6417.

56. Rojas, C. I. V.; Fine, J.; Slipchenko, L. V. Exchange-repulsion energy in QM/EFP. *Journal of Chemical Physics* **2018**, *149*, 094103.

57. Smith, Q. A.; Ruedenberg, K.; Gordon, M. S.; Slipchenko, L. V. The dispersion interaction between quantum mechanics and effective fragment potential molecules. *Journal of Chemical Physics* **2012**, *136*, 244107.

58. Hapka, M.; Przybytek, M.; Pernal, K. Symmetry-Adapted Perturbation Theory Based on Multiconfigurational Wave Function Description of Monomers. *Journal of Chemical Theory and Computation* **2021**, *17*, 5538–5555, PMID: 34517707.

59. Jangrouei, M. R.; Krzemińska, A.; Hapka, M.; Pastorczak, E.; Pernal, K. Dispersion Interactions in Exciton-Localized States. Theory and Applications to $\pi - \pi^*$ and $n - \pi^*$ Excited States. *Journal of Chemical Theory and Computation* **2022**, *18*, 3497–3511, PMID: 35587598.

60. Jeziorski, B.; Moszynski, R.; Szalewicz, K. Perturbation Theory Approach to Intermolecular Potential Energy Surfaces of van der Waals Complexes. *Chemical Reviews* **1994**, *94*, 1887–1930.

61. Szalewicz, K. Symmetry-adapted perturbation theory of intermolecular forces. *WIREs Computational Molecular Science* **2012**, *2*, 254–272.

62. Hancock, A. C.; Goerigk, L. Noncovalently bound excited-state dimers: a perspective on current time-dependent density functional theory approaches applied to aromatic excimer models. *RSC Advances* **2022**, *12*, 13014–13034.

63. Förster, T. Zwischenmolekulare Energiewanderung und Fluoreszenz. *Annalen der physik* **1948**, *437*, 55 – 75.

64. Chang, J. C. Monopole effects on electronic excitation interactions between large molecules. I. Application to energy transfer in chlorophylls. *The Journal of Chemical Physics* **1977**, *67*, 3901–3909.

65. Zanetti-Polzi, L.; Galdo, S. D.; Daidone, I.; D'Abramo, M.; Barone, V.; Aschi, M.; Amadei, A. Extending the perturbed matrix method beyond the dipolar approximation: comparison of different levels of theory. *Physical Chemistry Chemical Physics* **2018**, *20*, 24369 – 24378.

66. Fückel, B.; Köhn, A.; Harding, M. E.; Diezemann, G.; Hinze, G.; Basché, T.; Gauss, J. Theoretical investigation of electronic excitation energy transfer in bichromophoric assemblies. *The Journal of Chemical Physics* **2008**, *128*, 074505.

67. Krueger, B. P.; Scholes, G. D.; Fleming, G. R. Calculation of Couplings and Energy-Transfer Pathways between the Pigments of LH2 by the ab Initio Transition Density Cube Method. *The Journal of Physical Chemistry B* **1998**, *102*, 5378–5386.

68. Krueger, B. P. The Transition Density Cube method. `http://www.chem.hope.edu/~krieg/TDC/TDC_home.htm`, 1998; [Online; accessed Dec-2022].

69. Matthews, D. A.; Cheng, L.; Harding, M. E.; Lipparini, F.; Stopkowicz, S.; Jagau, T.-C.; Szalay, P. G.; Gauss, J.; Stanton, J. F. Coupled-cluster techniques for computational chemistry: The CFOUR program package. *The Journal of Chemical Physics* **2020**, *152*, 214108.

70. Stanton, J. F.; Gauss, J.; Cheng, L.; Harding, M. E.; Matthews, D. A.; Szalay, P. G. CFOUR, Coupled-Cluster techniques for Computational Chemistry, a quantum-chemical program package. With contributions from A.A. Auer, R.J. Bartlett, U. Benedikt, C. Berger, D.E. Bernholdt, Y.J. Bomble, O. Christiansen, F. Engel, R. Faber, M. Heckert, O. Heun, M. Hilgenberg, C. Huber, T.-C. Jagau, D. Jonsson, J. Jusélius, T. Kirsch, K. Klein, W.J. Lauderdale, F. Lipparini, T. Metzroth, L.A. Mück, D.P. O'Neill, D.R. Price, E. Prochnow, C. Puzzarini, K. Ruud, F. Schiffmann, W. Schwalbach, C. Simmons, S. Stopkowicz, A. Tajti, J. Vázquez, F. Wang, J.D.

Watts and the integral packages MOLECULE (J. Almlöf and P.R. Taylor), PROPS (P.R. Taylor), ABACUS (T. Helgaker, H.J. Aa. Jensen, P. Jørgensen, and J. Olsen), and ECP routines by A. V. Mitin and C. van Wüllen. For the current version, see http://www.cfour.de.

71. Li, X.; Parrish, R. M.; liu, F.; Schumacher, S. I. L. K.; Martinez, T. J. An Ab Initio Exciton Model Including Charge-Transfer Excited States. *Journal of Chemical Theory and Computation* **2017**, *13*, 3493 – 3504.

72. Curutchet, C.; Mennucci, B. Toward a molecular scale interpretation of excitation energy transfer in solvated bichromophoric systems. *Journal Of The American Chemical Society* **2005**, *127*, 16733–16744.

73. Hsu, C.-P.; Fleming, G. R.; Head-Gordon, M.; Head-Gordon, T. Excitation energy transfer in condensed media. *Journal of Chemical Physics* **2001**, *114*, 3065.

74. Dexter, D. L. A Theory of Sensitized Luminescence in Solids. *The Journal of Chemical Physics* **1953**, *21*, 836–850.

75. Förster, T. *Delocalized excitation and excitation transfer*; Modern Quantum Chemistry: Istanbul Lectures. Part III, Action of Light and Organic Crystals. Ed. O. Sinanoglu; Academic: New York, 1965.

76. Scholes, G. D. LONG-RANGE RESONANCE ENERGY TRANSFER IN MOLECULAR SYSTEMS. *Physical Chemistry* **2003**, *54*, 57–87.

77. Muñoz-Losa, A.; Curutchet, C.; Galván, I. F.; Mennucci, B. Quantum mechanical methods applied to excitation energy transfer: A comparative analysis on excitation energies and electronic couplings. *The Journal of Chemical Physics* **2008**, *129*, 034104.

78. Schreiber, M.; Silva, M. R. J.; Sauer, S. P. A.; Thiel, W. Benchmarks for electronically excited states: CASPT2, CC2, CCSD, and CC3. *The Journal of Chemical Physics* **2008**, *128*.

79. Christiansen, O.; Koch, H.; Jørgensen, P. The Second-order Approximate Coupled-Cluster Singles and Doubles Model CC2. *Chem. Phys. Lett.* **1995**, *243*, 409–418.

80. Schirmer, J.; Trofimov, A. B. Intermediate state representation approach to physical properties of electronically excited molecules. *J. Chem. Phys.* **2004**, *120*, 11449–11464.

81. Hellweg, A.; Grün, S. A.; Hättig, C. Benchmarking the performance of spin-component scaled CC2 in ground and electronically excited states. *Phys. Chem. Chem. Phys.* **2008**, *10*, 4119–4127.

82. Winter, N. O. C.; Hättig, C. Scaled opposite-spin CC2 for ground and excited states with fourth order scaling computational costs. *J. Chem. Phys.* **2011**, *134*, 184101.

83. Stanton, J. F.; Bartlett, R. J. The Equation of Motion Coupled-Cluster Method - A Systematic Biorthogonal Approach to Molecular-Excitation Energies, Transition-Probabilities, and Excited-State Properties. *J. Chem. Phys.* **1993**, *98*, 7029–7039.

84. Comeau, D. C.; Bartlett, R. J. The Equation-of-Motion Coupled-Cluster Method - Applications to Open-Shell and Closed-Shell Reference States. *Chem. Phys. Lett.* **1993**, *207*, 414–423.

85. Sinnokrot, M. O.; Sherrill, C. D. Highly accurate coupled cluster potential energy curves for the benzene dimer: sandwich, T-shaped, and parallel-displaced configurations. *The Journal of Physical Chemistry A* **2004**, *108*, 10200 – 10207.

86. Bartlett, R. J.; Purvis III, G. D. Molecular Applications of Coupled Cluster and Many-Body Perturbation Methods. *Phys. Scr.* **1980**, *21*, 255–265.

87. Dunning Jr, T. H. Gaussian basis sets for use in correlated molecular calculations. I. The atoms boron through neon and hydrogen. *The Journal of Chemical Physics* **1989**, *90*, 1007–1023.

88. Kendall, R. A.; Dunning, T. H.; Harrison, R. J. Electron-Affinities of the 1st-Row Atoms Revisited - Systematic Basis-Sets and Wave-Functions. *J. Chem. Phys.* **1992**, *96*, 6796–6806.

89. Boys, S.; Bernardi, F. The calculation of small molecular interactions by the differences of separate total energies. Some procedures with reduced errors. *Molecular Physics* **1970**, *19*, 553–566.

90. Cook, D. B.; Sordo, J. A.; Sordo, T. L. Some comments on the counterpoise correction for the basis set superposition error at the correlated level. *International Journal of Quantum Chemistry* **1993**, *48*, 375–384.

91. Burns, L. A.; Marshall, M. S.; Sherrill, C. D. Comparing Counterpoise-Corrected, Uncorrected, and Averaged Binding Energies for Benchmarking Noncovalent Interactions. *Journal of Chemical Theory and Computation* **2014**, *10*, 49–57.

92. Kristensen, K.; Ettenhuber, P.; Eriksen, J. J.; Jensen, F.; Jørgensen, P. The same number of optimized parameters scheme for determining intermolecular interaction energies. *The Journal of Chemical Physics* **2015**, *142*, 114116.

93. Aidas, K.; Angeli, C.; Bak, K. L.; Bakken, V.; Bast, R.; Boman, L.; Christiansen, O.; Cimiraglia, R.; Coriani, S.; Dahle, P.; Dalskov, E. K.; Ekström, U.; Enevoldsen, T.; Eriksen, J. J.; Ettenhuber, P.; Fernández, B.; Ferrighi, L.; Fliegl, H.; Frediani, L.; Hald, K.; Halkier, A.; Hättig, C.; Heiberg, H.; Helgaker, T.; Hennum, A. C.; Hettema, H.; Hjertenæs, E.; Høst, S.; Høyvik, I.-M.; Iozzi, M. F.; Jansík, B.; Jensen, H. J. Aa.; Jonsson, D.; Jørgensen, P.; Kauczor, J.; Kirpekar, S.; Kjærgaard, T.; Klopper, W.; Knecht, S.; Kobayashi, R.; Koch, H.; Kongsted, J.; Krapp, A.; Kristensen, K.; Ligabue, A.; Lutnæs, O. B.; Melo, J. I.; Mikkelsen, K. V.; Myhre, R. H.; Neiss, C.; Nielsen, C. B.; Norman, P.; Olsen, J.; Olsen, J. M. H.; Osted, A.; Packer, M. J.; Pawlowski, F.; Pedersen, T. B.; Provasi, P. F.; Reine, S.; Rinkevicius, Z.; Ruden, T. A.; Ruud, K.; Rybkin, V. V.; Sałek, P.; Samson, C. C. M.; de Merás, A. S.; Saue, T.; Sauer, S. P. A.; Schimmelpfennig, B.; Sneskov, K.; Steindal, A. H.; Sylvester-Hvid, K. O.; Taylor, P. R.; Teale, A. M.; Tellgren, E. I.; Tew, D. P.; Thorvaldsen, A. J.; Thøgersen, L.; Vahtras, O.; Watson, M. A.; Wilson, D. J. D.; Ziolkowski, M.; Ågren, H. The Dalton quantum chemistry program system. *WIREs Comput. Mol. Sci.* **2014**, *4*, 269–284.

94. Rocha-Rinza, T.; Vico, L. D.; Veryazov, V.; Roos, B. O. A theoretical study of singlet low-energy excited states of the benzene dimer. *Chemical Physics Letters* **2006**, *426*, 268–272.

95. Rocha-Rinza, T.; Christiansen, O. Linear response coupled cluster study of the benzene excimer. *Chemical Physics Letters* **2009**, *482*, 44–49.

96. Krueger, R. A.; Blanquart, G. Exciplex Stabilization in Asymmetric Acene Dimers. *The Journal of Physical Chemistry A* **2019**, *123*, 1796–1806.

97. Serrano-Andrés, L.; Serrano-Pérez, J. J. In *Handbook of Computational Chemistry*; Leszczynski, J., Kaczmarek-Kedziera, A., Puzyn, T., Papadopoulos, M. G., Reis, H., Shukla, M. K., Eds.; Springer International Publishing: Cham, 2017; pp 639–725.

98. Barca, G. M. J.; Bertoni, C.; Carrington, L.; Datta, D.; De Silva, N.; Deustua, J. E.; Fedorov, D. G.; Gour, J. R.; Gunina, A. O.; Guidez, E.; Harville, T.; Irle, S.; Ivanic, J.; Kowalski, K.; Leang, S. S.; Li, H.; Li, W.; Lutz, J. J.; Magoulas, I.; Mato, J.; Mironov, V.; Nakata, H.; Pham, B. Q.; Piecuch, P.; Poole, D.; Pruitt, S. R.; Rendell, A. P.; Roskop, L. B.; Ruedenberg, K.; Sattasathuchana, T.; Schmidt, M. W.; Shen, J.; Slipchenko, L.; Sosonkina, M.; Sundriyal, V.; Tiwari, A.; Galvez Vallejo, J. L.; Westheimer, B.; Wloch, M.; Xu, P.; Zahariev, F.; Gordon, M. S. Recent developments in the general atomic and molecular electronic structure system. *The Journal of Chemical Physics* **2020**, *152*, 154102.

99. Kállay, M.; Nagy, P. R.; Rolik, Z.; Mester, D.; Samu, G.; Csontos, J.; Csóka, J.; Szabó, B. P.; Gyevi-Nagy, L.; Ladjánszki, I.; Szegedy, L.; Ladóczki, B.; Petrov, K.; Farkas, M.; Mezei, P. D.; Hégely., B. Mrcc, a quantum chemical program suite. See also Z. Rolik, L. Szegedy, I. Ladjánszki, B. Ladóczki, and M. Kállay, J. Chem. Phys. 139, 094105 (2013), as well as: `www.mrcc.hu`.

100. Perdew, J. P.; Burke, K.; Ernzerhof, M. Generalized Gradient Approximation Made Simple. *Phys. Rev. Lett.* **1996**, *77*, 3865–3868.

101. The General Atomic and Molecular Electronic Structure System (GAMESS), user manual. `https://www.msg.chem.iastate.edu/gamess/documentation.html`, [Online; accessed Jan-2023].

102. Slipchenko, L. V.; Gordon, M. S. Electrostatic energy in the effective fragment potential method: Theory and application to benzene dimer. *Journal of Computational Chemistry* **2007**, *28*, 276–291.

103. Kánnár, D.; Szalay, P. G. Benchmarking Coupled Cluster Methods on Valence Singlet Excited States. *J. Chem. Theory Comput.* **2014**, *10*, 3757–3765.